

Original manuscript

## **Nuclear Morphometry using a Deep Learning-based Algorithm has Prognostic Relevance for Canine Cutaneous Mast Cell Tumors**

Andreas Haghofer <sup>1,2</sup>, Eda Parlak <sup>3</sup>, Alexander Bartel <sup>4</sup>, Taryn A. Donovan <sup>5</sup>, Charles-Antoine Assenmacher <sup>6</sup>, Pompei Bolfa <sup>7</sup>, Michael J. Dark <sup>8</sup>, Andrea Fuchs-Baumgartinger <sup>3</sup>, Andrea Klang <sup>3</sup>, Kathrin Jäger <sup>9</sup>, Robert Klopffleisch <sup>4</sup>, Sophie Merz <sup>10</sup>, Barbara Richter <sup>3</sup>, F. Yvonne Schulman <sup>11</sup>, Jonathan Ganz <sup>12</sup>, Josef Scharinger <sup>2</sup>, Marc Aubreville <sup>12</sup>, Stephan M. Winkler <sup>1</sup>, Matti Kiupel <sup>13</sup>, Christof A. Bertram <sup>3</sup>

<sup>1</sup> University of Applied Sciences Upper Austria, Hagenberg, Austria

<sup>2</sup> Johannes Kepler University, Linz, Austria

<sup>3</sup> University of Veterinary Medicine Vienna, Vienna, Austria

<sup>4</sup> Freie Universität Berlin, Berlin, Germany

<sup>5</sup> The Schwarzman Animal Medical Center, New York, USA

<sup>6</sup> University of Pennsylvania, Philadelphia, PA, USA

<sup>7</sup> Ross University School of Veterinary Medicine, Basseterre, St. Kitts

<sup>8</sup> University of Florida, Gainesville, FL, USA

<sup>9</sup> Laboklin GmbH & Co. KG, Bad Kissing, Germany

<sup>10</sup> IDEXX Vet Med Labor GmbH, Kornwestheim, Germany

<sup>11</sup> Heska, an Antech Company, Loveland, CO, USA

<sup>12</sup> Technische Hochschule Ingolstadt, Germany

<sup>13</sup> Michigan State University, Lansing, MI, USA

Corresponding author:

Christof Bertram, Institute of Pathology, University of Veterinary Medicine Vienna, Veterinärplatz 1, 1210 Vienna, Austria. Email: [Christof.bertram@vetmeduni.ac.at](mailto:Christof.bertram@vetmeduni.ac.at)

## Abstract

Variation in nuclear size and shape is an important criterion of malignancy for many tumor types; however, categorical estimates by pathologists have poor reproducibility. Measurements of nuclear characteristics (morphometry) can improve reproducibility, but manual methods are time consuming. In this study, we evaluated fully automated morphometry using a deep learning-based algorithm in 96 canine cutaneous mast cell tumors with information on patient survival. Algorithmic morphometry was compared with karyomegaly estimates by 11 pathologists, manual nuclear morphometry of 12 cells by 9 pathologists, and the mitotic count as a benchmark. The prognostic value of automated morphometry was high with an area under the ROC curve regarding the tumor-specific survival of 0.943 (95%CI: 0.889 – 0.996) for the standard deviation (SD) of nuclear area, which was higher than manual morphometry of all pathologists combined (0.868, 95%CI: 0.737 – 0.991) and the mitotic count (0.885, 95%CI: 0.765 - 1.00). At the proposed thresholds, the hazard ratio for algorithmic morphometry (SD of nuclear area  $\geq 9.0 \mu\text{m}^2$ ) was 18.3 (95%CI: 5.0 – 67.1), for manual morphometry (SD of nuclear area  $\geq 10.9 \mu\text{m}^2$ ) 9.0 (95%CI: 6.0 – 13.4), for karyomegaly estimates 7.6 (95%CI: 5.7 – 10.1), and for the mitotic count 30.5 (95%CI: 7.8 – 118.0). Inter-rater reproducibility for karyomegaly estimates was fair ( $k = 0.226$ ) with highly variable sensitivity/specificity values for the individual pathologists. Reproducibility for manual morphometry (SD of nuclear area) was good (ICC = 0.654). This study supports the use of algorithmic morphometry as a prognostic test to overcome the limitations of estimates and manual measurements.

## Keywords

Anisokaryosis, Artificial Intelligence, Computer Vision, Dog, Karyomegaly, Mast Cell Tumor, Mitotic Count, Tumor heterogeneity

## Introduction

Variation in nuclear size and shape of neoplastic cells is an important histologic criterion of malignancy, and various evaluation methods have been used in previous studies. The most practical method is categorical estimation by pathologists, most commonly evaluating anisokaryosis or nuclear pleomorphism. Anisokaryosis is defined as the variation of nuclear size of neoplastic cells, and nuclear pleomorphism describes the variation in nuclear size and shape. While these estimates have been shown to be relevant histologic prognostic tests for several animal tumors,<sup>15,28,31,34,37</sup> some studies suggest low inter- and intra-rater reproducibility.<sup>38,39</sup> For both methods, categories (such as mild, moderate, and severe) can only be vaguely defined and applications of the same thresholds between pathologists may be problematic. Another limitation is that estimates are based on categories that need to be defined before conducting a study, and thresholds are not based on a statistical association with patient outcome.

Alternatives to estimates are computerized measurements of nuclear size and/or shape (nuclear morphometry) in digital images, which can be either done by pathologists using a measurement software (manual morphometry)<sup>13,16,39</sup> or by image analysis algorithms (fully automated / algorithmic morphometry).<sup>1,14</sup> Morphometry can be based on two-dimensional measurements (nuclear area and shape),<sup>25,41</sup> or three-dimensional volume estimates based on stereological assumptions from two-dimensional histologic sections using point-sampled intercepts (volume-weighted mean nuclear volume).<sup>13,39</sup> Besides an assumed higher degree of reproducibility as compared to estimates, a potential benefit is the output of numerical values, which allows statistical determination of meaningful prognostic thresholds at the desired sensitivity and specificity trade off. However, manual measurements by pathologists are time consuming and, thus, difficult to conduct in a routine diagnostic setting. A time investment of 10-15 minutes has been reported for 75 and 166 ( $\pm$  66 SD) point-sampled intercept measurements.<sup>13,39</sup> In contrast, algorithms using state-of-the-art deep learning models are capable of eliminating human labor for these tasks and are very promising for quantitative evaluation of tumor markers.<sup>9,30</sup> Fully-automated nuclear morphometry can be done by post-processing of algorithmic nuclear segmentation (demarcation of all pixels representing the nuclei) masks (algorithmic output).<sup>14</sup>

Aside from morphometry based on nuclear segmentation, additional image analysis approaches have been used for automated evaluation of nuclear features: 1) image classification that categorizes images into tiers of anisokaryosis;<sup>27</sup> and 2) regression analysis that generates a continuous score based on the anisokaryosis tiers.<sup>29</sup> While all approaches achieve the goal of improving rater reproducibility by removing rater subjectivity, automated nuclear morphometry has several advantages as it is a quantitative and a very adaptable method. With two-dimensional morphometry, several nuclear characteristics can be evaluated individually or in combination at any desired prognostic threshold (see materials and methods section), while classification and regression approaches are restricted to the predefined classes of morphological patterns. Additionally, segmentation masks can be easily displayed as an overlay on the histological image, which allows visual verification of algorithmic performance to ensure reliability of the prognostic interpretation. Segmentation models can probably also be developed in a more consistent manner due to the nature of their ground truth data used for training (accurate nuclear contour annotations), which are, however, more time consuming to create when compared to the other approaches with one label (anisokaryosis estimates) per image.

Canine cutaneous mast cell tumors (ccMCT) are one of the most pertinent skin tumors in dogs for possible application of these solutions due to their high frequency and malignant potential.<sup>22</sup> While studies on prognostic parameters for this tumor type are extensive in the veterinary oncologic literature, including the mitotic count and two multi-parameter grading systems first published in 1984 and 2011,<sup>5,8,10,20,23,32,36</sup> further relatively inexpensive and easy quantitative tests are needed to improve the prognostic ability of routine histopathologic assessment. Interestingly, despite their inclusion in the multi-parameter grading systems,<sup>23,32</sup> the prognostic value of histologic estimates of nuclear characteristics has rarely been investigated in ccMCT.<sup>12,40</sup> In an attempt to provide more objective criteria, the 2011 two-tier grading system defined a tumor as having karyomegaly if "the nuclear diameters of at least 10% of neoplastic mast cells vary by at least two-fold".<sup>23</sup> However, that definition of karyomegaly (origin of the word from ancient greek for nuclear enlargement) actually reflects anisokaryosis (variation in nuclear size), doesn't necessarily require abnormally enlarged nuclei, and would not be fulfilled when all neoplastic cells are karyomegalic. Further, a significant association of karyomegaly as a solitary parameter with survival has not been shown to date.<sup>12</sup> The prognostic value of manual nuclear morphometry of ccMCT has rarely been investigated for histologic<sup>13</sup> and cytologic ccMCT specimens<sup>41</sup> using either the two- and three-dimensional approaches. Fully automated solutions for nuclear morphometry have not been studied for ccMCT or any other animal tumors thus far, as opposed to human tumors.<sup>1,14,44</sup> In addition, the variation of nuclear characteristics between different tumor areas in histological sections (tumor heterogeneity) has not been evaluated for ccMCT. This information on tumor heterogeneity is relevant for deciding best sampling strategies of regions of interest used for image analysis.

The primary objective of this study was to investigate automated nuclear morphometry for ccMCT and compare it with simple methods of nuclear size evaluation (estimation and measurements by pathologists) and the mitotic count as a benchmark. In this study the measurement error, prognostic utility and reproducibility of each nuclear evaluation method are investigated. A second objective was to evaluate the heterogeneity of nuclear size in different tumor areas.

## Material and Methods

### Material

Two separate sets of histological images with associated data, a ground truth dataset for nuclei segmentation and a dataset with survival outcome, were used in this study. The ground truth dataset was primarily used to train, validate and test the deep learning-based algorithm (fully automated morphometry) and the outcome dataset was used to apply and determine the prognostic value of the nuclear evaluation methods (see method section). For both independent datasets, histological sections of ccMCTs stained by hematoxylin and eosin were digitized with the Panoramic Scan II (3DHistech, Hungary) whole slide image scanner at default settings with a scan magnification of 400x (resolution of 0.25  $\mu\text{m}$  / pixel). Each whole slide image (WSI) represented a different ccMCT case. Using the software SlideRunner,<sup>2</sup> a variable number of ROI within each WSI (see below) were cropped and exported as TIFF files using lossless compression. Each ROI had a size of 0.1185 mm<sup>2</sup> (equivalent to 0.5 standard high power fields<sup>30</sup>) and an aspect ratio of 4:3. The ROI selection at low

magnification was designed to include a representative tumor region without paying particular attention to nuclear characteristics.

### **Ground Truth Dataset**

CcMCT cases were retrieved from the diagnostic archive of four veterinary pathology laboratories (Michigan State University, MSU, N = 21; The Schwarzman Animal Medical Center New York, N = 14; Freie University Berlin, N = 14; Vetmeduni Vienna, N = 15) with equal numbers of high- and low-grade tumors based on the 2011 histological grading system.<sup>23</sup> For the samples from MSU, two ROI per WSI were used, and for the samples from other laboratories, one ROI per WSI was used. While the cases from MSU were the target domain for application of the algorithm (see outcome dataset), the other laboratories were used to increase robustness of the derived algorithm. Using the software SlideRunner,<sup>2,18</sup> one author (EP) carefully delineated the contours of the nuclear membrane of all mast cells present in these 85 images using the polygon annotation tool. The final dataset comprised 40,542 ground truth annotations (average per ROI: 455, range: 107 – 1049). The images were randomly assigned to the algorithm training subset (N = 61), validation subset (N = 11) and the test subset (N = 13), while the two images per case from the MSU were always assigned to the same subset. The annotations of the test subset were morphometrically measured (subsequently referred to as ground truth measurements) as listed in Table 1 and described for the algorithm below.

### **Outcome Dataset**

The outcome dataset consists of 96 cases (one tumor per patient) with known follow-up on patient survival. Histological sections were produced at MSU. Information on patient follow up (date of surgery, date of death and suspected cause of death) was collected through a survey sent to the submitters of the surgical tissue samples. Patients that were lost to follow-up before 12 months after surgical excision of the ccMCT or were treated by systemic or radiation therapy were excluded. Postmortem examinations to verify the tumor burden were not available for any case.

For larger tumors (N = 91), 5 ROI in different tumor locations at the periphery and center were selected. For smaller tumors, sections in which the 5 ROI could not be placed without overlap (N = 5), the maximum number of non-overlapping ROI (3, N = 1; or 4, N = 4) was chosen.

## **Methods**

For this study, different methods of nuclear size and shape evaluation encompassed:

- Deep learning-based segmentation algorithm for fully automated morphometry of nuclear size (area) and shape (eccentricity and solidity).
- Pathologists' evaluation (N = 11 and 9) at two separate time points:
  - Anisokaryosis estimates by pathologists based on a three-tier (referred to as three-tier anisokaryosis) and a two-tier (referred to as karyomegaly) classification scheme.
  - Nuclear size measurements of 12 representative nuclei (manual morphometry).

As a benchmark for the prognostic value of the nuclear evaluation methods, the mitotic count (MC) was determined. The methods of each test are specified in the following sections.

### **Supervised Deep Learning-Based Algorithm (Fully Automated Morphometry)**

Using the PyTorch lightning framework,<sup>18</sup> we developed a Unet ++<sup>45</sup>-based segmentation model with RegNetY120 backbone<sup>35</sup> of the segmentation models package<sup>21</sup> to create binary masks where pixels corresponding to the nuclei of the initial slide image are depicted as positive foreground (ones) in front of a negative background (zeros). We trained our model for 2,000 epochs using the training and validation subsets of the ground truth dataset. During each epoch, all 61 training samples are split into batches of eight samples. Processing one batch per step, we got 7.625 training steps, resulting in seven full batches and one batch with only five samples. The final model was selected as the best out of all processed epochs based on the validation loss (focal loss, evaluated on the validation subset). We applied data augmentation including extension techniques to the training data to regularize the training process (for the validation data, we only applied data extension without augmentation). The data augmentation methods used consisted of color and contrast adjustments combined with various distortion methods like elastic-, optical-, grid-distortion, and methods like shifting, scaling, and rotation to increase the variation in the available images to decrease overfitting and the impact of domain shift due to different imaging setups.

To extend our dataset, we multiplied the number of steps per epoch by a factor of 10, resulting in ~77 training steps. Using the same calculation, we also got 14 validation steps at the end of each epoch. In order to generate the necessary images for the extended number of batches, we used image cropping. This involves randomly selecting image regions of 512x512 pixels out of the original dataset, with images of 1601x1201 pixels, until the required number of crops is reached. Exclusively for the training steps, we resampled new crops for every epoch and applied data augmentation to each crop.

After applying the deep learning model for segmentation of individual nuclei, we used a filter mechanism as post-processing for the exclusion of objects that did not represent a valid nucleus. This filter uses an approximation for comparing the mean diameter of the segmented object with a defined diameter. Thus, we excluded objects with fewer pixels than a circle with a minimum diameter of 3 $\mu$ m. This approximation excludes objects within our segmentation masks that are too small and do not represent complete and valid nuclei.

Subsequent to segmentation and filtering of the individual mast cell nuclei, different morphometric parameters were calculated for each case as listed in Table 1 (algorithmic morphometry). These included different characteristics of the probability density function, such as mean and standard deviation (SD), of nuclear area and shape. Nuclear area was defined by the number of pixels within the segmented objects and subsequent conversion into  $\mu$ m<sup>2</sup> based on the scan resolution. The SD of the nuclear area reflects the variation of the nuclear size and thus was used as the primary parameter to compare with the three-tier anisokaryosis estimates by pathologists (see below). To approximate the two-tier system definition for karyomegaly, “nuclear diameters of at least 10% of neoplastic mast cells [i.e., proportion of large nuclei] vary

by at least two-fold [i.e., extent of nuclear size difference]<sup>23</sup>, we evaluated two morphometric parameters. The proportion of abnormally enlarged (karyomegalic) cells was calculated by the number of nuclei above a specific size (case-independent reference size as defined in the next sentence) divided by the number of all tumor nuclei detected. The case-independent threshold for large nuclei was an area of  $>50.3 \mu\text{m}^2$  (two times the median area of all the annotated nuclei in the training/validation dataset) or  $>37.8 \mu\text{m}^2$  (the 90<sup>th</sup> percentile of the annotated nuclei). The extent of nuclear size variation was determined by the 90<sup>th</sup> percentile divided by the median, representing the factor by which the largest 10% of nuclei, i.e., potentially karyomegalic cells, differ from the median nuclear size of the same tumor (case-specific reference size). Instead of using the diameter according to the karyomegaly definition used in the two-tier system, we based our calculations on the nuclear area, as an increase of the diameter is not proportional to the actual increase of nuclear size and a nuclear diameter is not representative of size for oval nuclei.

As indicators of nuclear shape, we measured eccentricity and solidity, as implemented in the scikit-image framework.<sup>43</sup> The eccentricity measure is used to evaluate the roundness of the detected object. It is calculated by the ratio of the distance between the focal points of an ellipse over the major axis length. The closer this ratio is to 1, the more elongated the shape is. The closer the ratio is to 0, the more circular the shape is. For the calculation of the solidity measure, we used the ratio of the detected object area compared to the resulting convex hull of this area. A solidity value of 1 indicates that the detected pixel area has exactly the same size as its convex hull. The closer this value is to 0, the more indentations are present and/or the larger the indentations are, corresponding to the bizarre nuclei definition of the 2011 grading system.<sup>23</sup> Nuclear indentation thresholds evaluated were  $<0.913$ ,  $<0.936$ ,  $<0.943$ , representing the 2nd, 5th, and 10th percentile, respectively, of the training and validation dataset. The percentage of indented nuclei over all detected nuclei was calculated. For calculation of the prognostic value of mean solidity, the direction of the values was inverted (i.e., higher degree of nuclear indentations are represented by larger values) by subtracting the mean solidity value from 1 for each case.

The developed algorithm was used to analyze the images of the test subset of the ground truth dataset and the outcome dataset. For the outcome cases, calculations were done for each ROI separately and averaged for all ROI per case.

**Table 1.** List of parameters for algorithmic morphometry evaluated in this study.

<b>Feature</b>	<b>Measurement</b>	<b>Parameters</b>
Size	Area (in $\mu\text{m}^2$ )	Mean, median, standard deviation (SD), 90 <sup>th</sup> percentile (90 <sup>th</sup> P), 90 <sup>th</sup> P / median, mean of the largest 10% of the nuclei, percentage of large nuclei ( $>37.8 \mu\text{m}^2$ or $>50.3 \mu\text{m}^2$ ), skewness (asymmetry of the data distribution)
Size	Eccentricity	Mean, SD, skewness
	Solidity	Mean, SD, Percentage of nuclei with indentation (solidity $<0.913$ ), skewness

### **Pathologists' Evaluation of Nuclear Size**

Eleven veterinary pathologists from 9 different laboratories participated in this study. Study participation consisted of two time points with a wash out time of at least 2 weeks. For time point 1 (completed by all participants), pathologists were asked to estimate the degree of anisokaryosis using two systems (see below) for the cases of the outcome dataset. For time point 2 (completed by 9 participants), pathologists were instructed to estimate the degree of anisokaryosis a second time and to measure 12 neoplastic mast cell nuclei (manual morphometry, see below) for each tumor in the test subset of the ground truth dataset and the outcome dataset. Images were provided to the pathologists through the online annotation platform EXACT.<sup>26</sup> The images from the 3-5 ROI of each case of the outcome dataset were stitched to an image panel and separated by a thick, black line to allow simultaneous viewing. Pathologists were blinded to the assessment by the other pathologists, algorithmic predictions, and outcome information. After the experiment, the participants were anonymized by randomly assigning an identification number (P1 – P11).

### **Anisokaryosis Estimates**

Two classification schemes (two- and three-tier) for anisokaryosis estimation were applied by the pathologists for each case at two time points, resulting in 1,920 data points for the outcome dataset and 117 data points for the test subset of the ground truth dataset. First, the three-tier anisokaryosis system consisted of the following categories: 1) none to mild, 2) moderate, and 3) severe variation in nuclear size of neoplastic mast cells. These stratifications were intentionally vaguely defined as this is common practice in current literature. Secondly, karyomegaly was assessed according to the definition given by Kiupel et al. for the two-tier MCT grading system,<sup>23</sup> “nuclear diameters of at least 10% of neoplastic mast cells vary by at least two-fold,” as: 1) absent or 2) present.

### **Nuclear Size Measurements (Manual Morphometry)**

For time point 2, pathologists were asked to measure 12 neoplastic mast cell nuclei per case (Fig. 1). The images from the test subset of the ground truth dataset were analyzed first (resulting in a total of 1,407 annotations by 9 pathologists, three images had 13 annotations by one pathologist), and subsequently, the images of the outcome dataset were evaluated (resulting in a total of 10,368 annotations). Pathologists were asked to use the ROI of the outcome cases with the presumed highest degree of anisokaryosis. For cases with notable nuclear size differences, participants were instructed to select 4 nuclei with a small, intermediate, and large area each. The polygon annotation tool in Exact<sup>26</sup> was used to outline the neoplastic nuclei. Based on the annotations, the mean, SD, and maximum nuclear area were calculated for each case and pathologist.

### **Mitotic Count (Benchmark) and Histologic Grade**

The mitotic count (MC) is probably the single most important prognostic histological parameter for ccMCT.<sup>8,22</sup> Thus, we used this test as a benchmark of prognostic relevance to compare with the nuclear evaluation methods (outcome dataset). We consider the histologic grading schemes<sup>23,32</sup> to be a less appropriate reference test for



this study because these systems combine nuclear characteristics with other morphologic criteria; thus, they are theoretically superior to a single morphometric parameter. As the grades are categorical values, some statistical tests for evaluation of the prognostic relevance (see below) are not possible as compared to numerical tests such as the MC and nuclear morphometry.

The MC was determined by one pathologist (CAB) in the WSIs of the outcome dataset according to current guidelines.<sup>30</sup> The software SlideRunner<sup>2</sup> with a plug-in for an rectangular bounding box overlay (4:3 ratio, area of exactly 2.37 mm<sup>2</sup>) was used, as previously described.<sup>6</sup> This area box was placed in a mitotic hotspot location, which was selected based on the impression of mitotic activity evaluated in several tumor areas. Regions with widespread necrosis, severe inflammation, low tumor cell density, poor cell preservation, and extensive artifacts were excluded, if possible. All mitotic figures (according to published definitions<sup>17</sup>) within this hotspot area were enumerated by screening these areas at high magnification two times.

The two-tier grading system was determined by one pathologist (CAB) for the cases of the outcome dataset according to the published criteria.<sup>23</sup> The same MC as determined above was used for grading and the other parameters were determined in the WSIs.

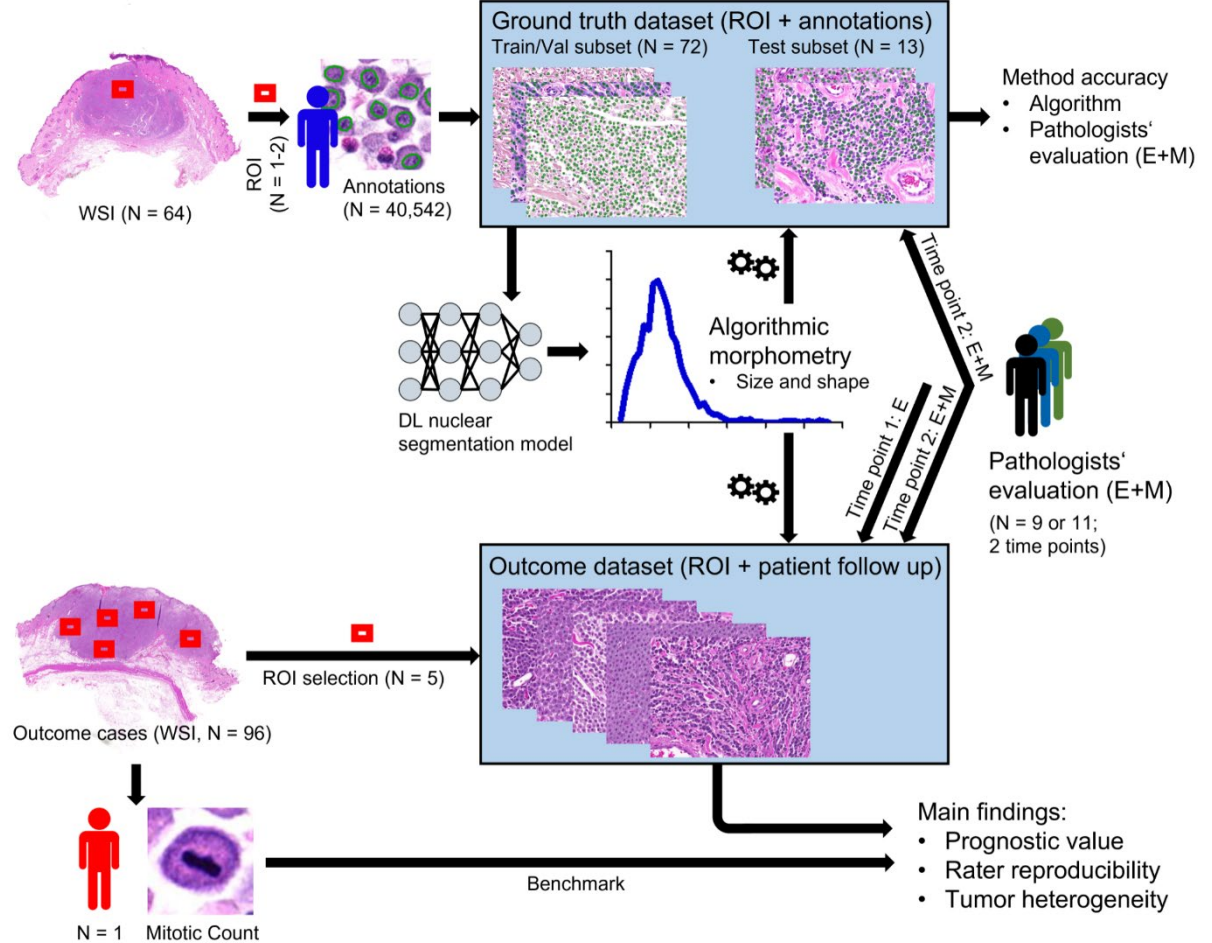


**Figure 1.** Overview of the study design. Two different sets of histological images with associated data, the ground truth dataset and the outcome dataset, were used to investigate different evaluation methods for nuclear size and shape.

DL, deep learning-based; ROI, regions of interest; WSI, whole slide images; E, anisokaryosis estimates; M, nuclear size measurements, Train/Val subset, training and validation subset.

## Statistical Analysis

Statistical analysis and graph creation was performed by GraphPad Prism version 5.0 (GraphPad Software, San Diego, CA), IBM SPSS Statistics version 29.0 (IBM Corporation, Armonk, NY) and R version 4.2.2 (R Foundation, Vienna, Austria).

### **Test accuracy (ground truth dataset) and correlation (outcome dataset)**

Our workflow's accuracy was determined on 13 images from the test subset of the ground truth dataset. Segmentation performance of the deep learning model was determined by the proportion of overlap between the model predictions and the ground truth annotations (intersection over union, also known as Jaccard index). Measurement errors of algorithmic and manual measurements for the entire image were determined by comparison to the ground truth measurement using the root mean squared error (RMSE). Algorithmic and manual measurements, and pathologists' estimates were compared with the ground truth measurements using scatterplots.

The correlation of the algorithmic morphometric parameters was analyzed on the outcome dataset using Pearson's method.

### **Prognostic value (outcome dataset)**

The outcome metrics primarily evaluated in this study (outcome dataset) were tumor-related mortality at any time of the follow up period and tumor-specific survival time. Dogs that died due to other causes (not considered ccMCT-related by the clinician) were grouped with cases that survived the follow-up period (ROC curves, scatter plots, sensitivity and specificity) or were censored (Kaplan Meier curves and hazard ratios). The bias of this outcome metric is the variable follow-up period between cases without reported death (minimum of 12 months) and the lack of conclusive proof of the cause of death. It can't be ruled out that tumor-related mortality was missed in a few cases with a relatively short follow-up period, while acknowledging that most ccMCT patients that survive the first 12 months will die from other causes. To eliminate the bias of a variable follow-up period and unproven cause of death, tumor-specific mortality and overall mortality within the first 12 months of the follow-up period were used as alternative outcome metrics. Overall death was defined as the occurrence of death regardless of the cause of death.

Numerical tests (algorithmic and manual morphometry and MC) were analyzed by receiver operating characteristic (ROC) curves (plotting sensitivity against specificity for numerous thresholds) and the area under the ROC curve (AUC) with 95% confidence intervals (95% CI). The distribution of the algorithmic measurements and the MC were displayed in scatter plots comparing cases with tumor-related mortality and other cases. Numerical tests with an AUC  $\geq 0.700$  were dichotomized by thresholds, resulting in uniform sensitivity value for the different tests, which allows comparison of the associated specificity values. For the MC, the threshold proposed by Romansik et al.<sup>36</sup> was used to group cases with values of 0-5 and  $\geq 6$ . The range of the morphometric measurements were divided into 200 intervals (thresholds increased by 0.5% steps) and two thresholds leading to a sensitivity of 76.9% (threshold 1; 10 true positive cases, TP, and 3 false negative cases, FN; represents the sensitivity value for the MC), and 53.8% (threshold 2; 7 TP, 6 FN) were selected.

If multiple cut-off values resulted in the desired sensitivity value, the highest value was picked.

With the categorical data (dichotomized numerical tests and pathologists' estimates), Kaplan Meier curves, hazard ratios with 95% CI (univariate cox regression), as well as sensitivity (Sen, also known as recall), specificity (Sp) and precision (Pre, also known as positive predictive value) were calculated.

The pathologists' measurements were analyzed individually, averaged, and were combined (repeated measure data), when reasonable. For combined data, bootstrapping (AUC values) or a mixed model (cox regression) were used to calculate 95% CIs.

### **Rater reproducibility (outcome dataset)**

Rater reproducibility was determined for the cases of the outcome dataset. For categorical estimates, inter- and intra-rater reproducibility was determined by Light's Kappa and weighted Cohens Kappa (k). The level of agreement was interpreted as poor = 0, slight = 0.01–0.20, fair = 0.21–0.40, moderate = 0.41–0.60, substantial = 0.61–0.80, and almost perfect = 0.81–1.00.<sup>19</sup> For pathologists' measurements, inter-rater agreement was measured by the intraclass correlation coefficient (ICC; 2-way agreement, single measures, random) with the following interpretation: poor = 0–0.39, fair = 0.40–0.59, good = 0.6–0.74, and excellent = 0.75–1.00.<sup>19</sup> To compare the estimate categories assigned by each pathologist with the actual SD area (algorithmic morphometry) of the individual case, linear regression was used.

### **Intra-tumoral Heterogeneity (outcome dataset)**

Heterogeneity was evaluated for fully automated morphometric measurements between the different ROI per case using the outcome dataset. The difference between the 3-5 ROI was determined by the coefficient of variation (SD / mean). The influence of the number of ROI used for prognostic evaluation was determined by the AUC calculated from the mean measurements of 1, 2, 3, 4 and 5 ROI based on their order of selection within the WSI (see material section). Tumor heterogeneity as a prognostic test was defined by the SD between the 3-5 ROI and by the proportion of ROI with a morphometric measurement above threshold 1 (defined as a hotspot) over all evaluated ROI.

## **Results**

### **Test accuracy and correlation**

The segmentation model had a high performance with an intersection over union of 0.806 (Supplemental Fig. S1). Errors (RMSE) in the algorithmic measurements were considered acceptable with the exceptions of SD of eccentricity, percentage of nuclei with indentation, and the skewness measurements (Supplemental Table S1 and Fig. S2). The measurement errors for the pathologists were generally larger than the algorithmic errors with a tendency for higher values for all pathologists (Supplemental Table S2 and S3 and Figure S3 and S4). Higher categories of three-tier anisokaryosis and karyomegaly were more commonly assigned to cases with higher SD of nuclear

area, but with marked inconsistency between cases and pathologists (Supplemental Figure S3).

Most algorithmic parameters of nuclear area had a very strong correlation with each other including the 90<sup>th</sup> percentile and median with a correlation coefficient of 0.970 (Supplemental Table S4, Figure S5). SD of eccentricity and solidity moderately correlated with the nuclear area parameters with coefficients ranging between 0.404 to 0.674.

### **Prognostic Value**

Of the 96 cases (78 low-grade cases and 18 high-grade cases) included in the outcome dataset, death was attributed to the ccMCT in 13 cases with a median survival time of 4.3 months (range: 0.5 - 24). Other cases (N = 83) were lost to follow-up (N = 72) with a median follow-up period of 24 months (range: 12 - 45.3 months) or were reported to have died due to ccMCT-unrelated causes (N = 11) with a median survival time of 8.5 months (range: 0.2 - 29.7). At 12 months after surgical removal, 10 had died due to ccMCT-related and 6 due to ccMCT-unrelated causes. The demographic characteristics of this study population are described in the supplemental material.

The deep learning-based algorithm detected an average of 373.67 (range: 120–822) segmented nuclei per ROI of the outcome dataset. Algorithmic nuclear area measurements based on these segmented nuclei achieved high AUC values regarding tumor-related mortality (Figure 2, Supplemental Table S5), most of which were above the MC (benchmark) with an AUC of 0.885 (95%CI: 0.765 - 1.00,  $p < 0.001$ ). On the other hand, algorithmic shape measurements had AUC values below the benchmark, while mean shape values did not provide any prognostic information (AUC values close to 0.5). Similar observations were made regarding tumor-related mortality and overall mortality at 12 months after surgery (Supplemental Table S6 and S7). The average AUC of the pathologists' measurements were around the benchmark with some variability between the individual pathologists ranging between 0.857 to 0.957 for the mean area, 0.823 to 0.960 for the SD of nuclear area and 0.817 to 0.956 for the maximum area (Supplemental Table S8).

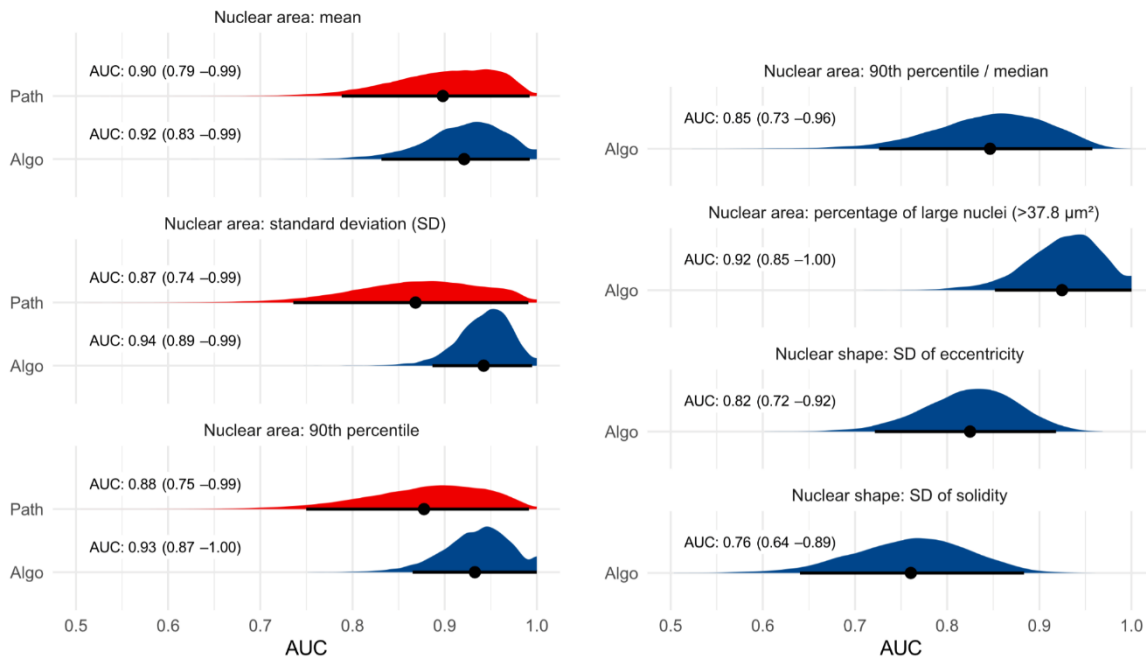


**Figure 2.** Graphical illustration of the AUC (point estimator, black dot) with its 95% confidence intervals (black line) and probability density function (red and blue areas) using bootstrapping for different nuclear morphometry parameters regarding tumor-specific survival. Algorithmic morphometry (Algo) is displayed in blue and manual morphometry by pathologists (Path) in red density functions.

Comparing the two outcome groups (tumor-related death vs. other) shows that the algorithmic SD of area measurements is able to distinguish patient outcome at a high sensitivity (threshold 1) or specificity (threshold 2), depending on the selected threshold (Fig. 3). Scatterplots for the other parameters of algorithmic nuclear morphometry and MC are provided in Supplemental Fig. S6 – S8. The specificity and precision values based on threshold 1 are provided in Table 2 for algorithmic and manual SDs of area measurements, revealing a high performance of the algorithm and high variability between the pathologists in the threshold required to obtain the same sensitivity values. For SD of nuclear area based on algorithmic morphometry, a tumor-specific death rate of 3.9% (false omission rate) and 52.6% (precision) was determined for cases below and above the threshold of  $\geq 9.0 \mu\text{m}^2$ , respectively (Supplemental Figure S6B). Classification results of further morphometric parameters are provided in Supplemental Table S9-S11, and the variability of manual morphometry between pathologists is summarized in Supplemental Fig. S9. The categorical anisokaryosis estimates by pathologists resulted in highly variable sensitivity (Sen) and specificity (Sp) values ranging between Sen = 100% / Sp = 4.8% (pathologist 8) to Sen = 46.2% / Sp = 98.8% (pathologist 7) for anisokaryosis 1 vs. 2 and 3, between Sen = 84.6% / Sp = 69.9% (pathologist 5) to Sen = 0% / Sp = 100% (pathologist 1) for anisokaryosis 1 and 2 vs 3, and between Sen = 92.3% / Sp = 31.3% (pathologist 11) to Sen = 0% / Sp = 98.8% (pathologist 5) for karyomegaly (Fig. 4; Supplemental Table S12 and S13). Almost all pathologists are below the algorithmic ROC curve (Fig. 4). As compared to the MC (Sen = 79.6%, Sp = 92.8%), the sensitivity was slightly higher for the 2011 two-tier histologic grade (Sen = 84.6%, Sp = 91.6%) due to the combination with the further nuclear characteristics.

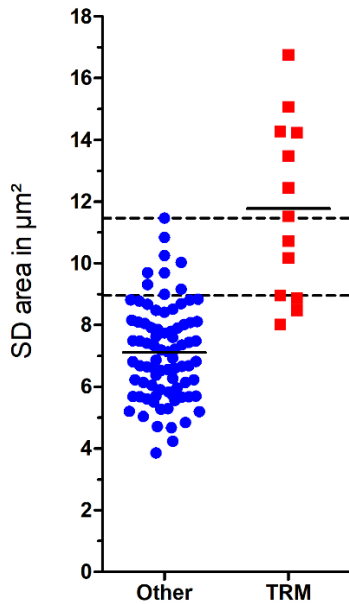


**Figure 3.** Scatterplot for standard deviation of nuclear area (SD area) measured by fully automated morphometry comparing cases with tumor-related mortality (TRM) with others (survived follow-up period or died due to tumor-unrelated cause). The lower broken line represents threshold 1 ( $9.0 \mu\text{m}^2$ ; sensitivity: 76.9%, specificity: 89.2%) and the upper broken line represents threshold 2 ( $11.5 \mu\text{m}^2$ ; sensitivity: 53.8%, specificity: 100%). The short solid lines represent the mean of the measurement of the respective outcome group.

**Table 2.** Sensitivity, specificity, and precision regarding tumor-related mortality for the mitotic count (benchmark) and standard deviation (SD) of nuclear area measured by algorithmic and manual (by the 9 pathologists, P) morphometry. The classification threshold is adapted to result in a sensitivity value of 76.9% for all tests.

Method	Parameter	Threshold	Sensitivity	Specificity	Precision
Reference	Mitotic count	$\geq 6$	76.9%	92.8%	62.5%
Algorithm	SD of nuclear area	$\geq 9.0 \mu\text{m}^2$	76.9%	89.2%	52.6%
P1		$\geq 8.0 \mu\text{m}^2$	76.9%	84.3%	43.5%
P2		$\geq 9.8 \mu\text{m}^2$	76.9%	84.3%	43.5%
P3		$\geq 10.9 \mu\text{m}^2$	76.9%	88.0%	50.0%
P5		$\geq 13.4 \mu\text{m}^2$	76.9%	86.7%	47.6%
P6		$\geq 8.5 \mu\text{m}^2$	76.9%	69.9%	28.6%
P7		$\geq 12.2 \mu\text{m}^2$	76.9%	95.2%	71.4%
P8		$\geq 10.5 \mu\text{m}^2$	76.9%	84.3%	43.5%
P10		$\geq 14.0 \mu\text{m}^2$	76.9%	90.4%	55.6%
P11		$\geq 12.2 \mu\text{m}^2$	76.9%	84.3%	43.5%

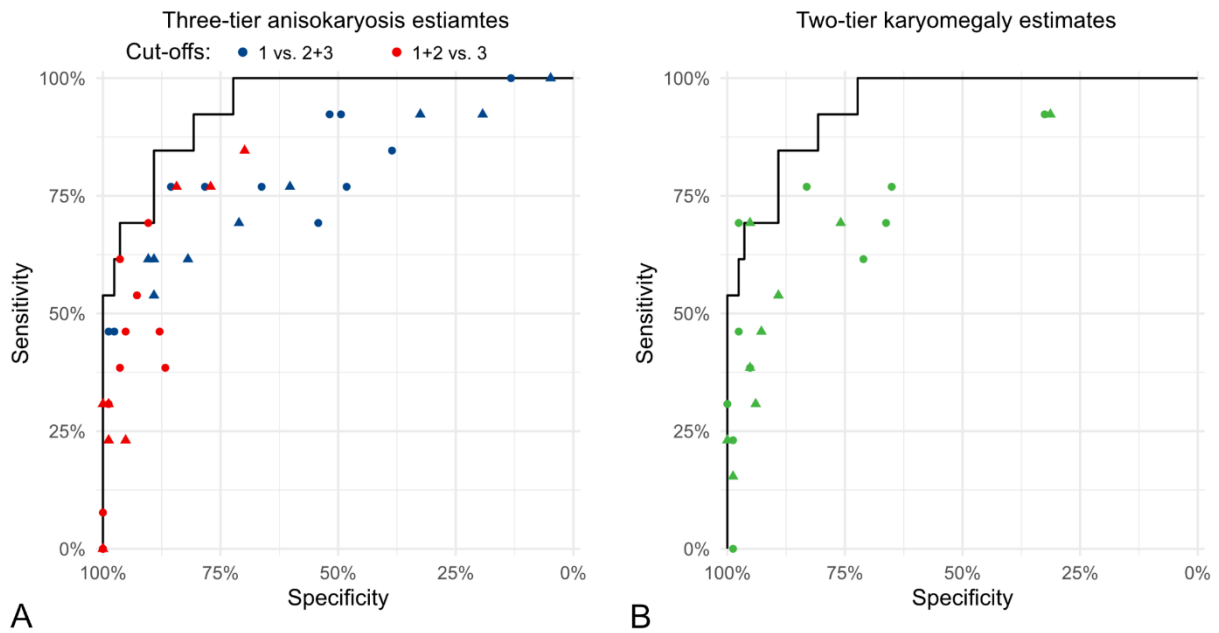


**Figure 4.** Comparison of the pathologists' sensitivity and specificity values for anisokaryosis estimates of time point 1 (dots) and 2 (triangle) regarding tumor-related mortality. The solid line in both graphs represents the same ROC curve for SD area measured by the deep learning-based algorithm. **A)** Pathologists' estimates (dots and triangles) based on the three-tier anisokaryosis (1: none to mild, 2: moderate or 3: severe) approach. Two of the three categories are combined into none to moderate vs. severe (red symbols) and none to mild vs. moderate to severe (blue symbols) anisokaryosis. **B)** Pathologists' estimates by the karyomegaly definition (green symbols).

Kaplan-Meier curves and hazard ratios determined that patient survival time was significantly different for cases with low versus high anisokaryosis based on threshold 1 for nuclear morphometry and the predefined categories of the estimates (Fig. 5; Supplemental Fig. S10-S12 and Table S14-S16). The hazard ratios of the morphometric size measurements were higher than those for the shape measurements (Supplemental Table S14); however, both were lower than the MC (benchmark) or histologic grading system with a value of 30.5 (95%CI: 7.8 – 118.0,  $p < 0.001$ ; Supplemental Fig. 13) or 46.5 (95%CI: 9.6 – 223.3,  $p < 0.001$ ), respectively.

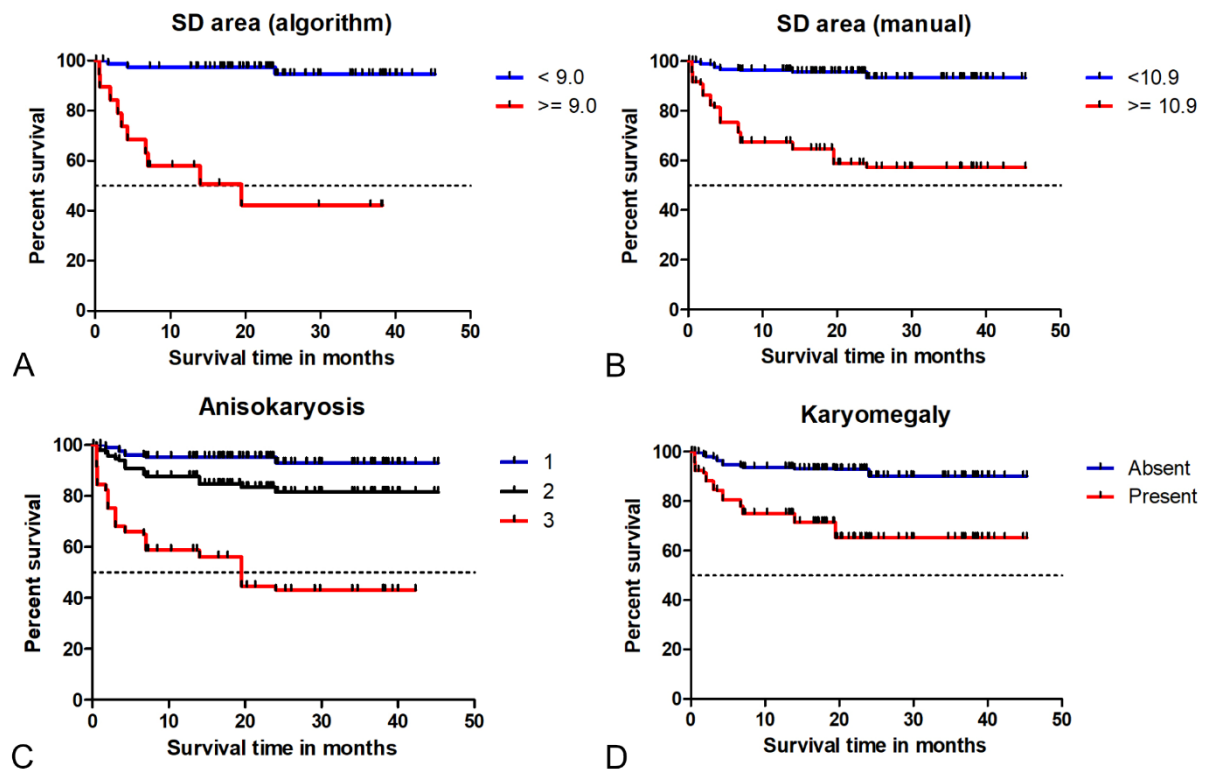


**Figure 5.** Kaplan Meier curves regarding tumor-specific survival time for different tests on nuclear size evaluation. **A)** standard deviation (SD) of nuclear area measured by algorithmic morphometry. The hazard ratio for this test is 18.3 (95% CI: 5.0 – 67.1,  $p < 0.001$ ). **B)** SD of nuclear area measured by manual morphometry (combined data of all 9 pathologists). The hazard ratio for this test is 9.0 (95% CI: 6.0 – 13.4,  $p < 0.001$ ). **C)** Three-tier anisokaryosis estimates (combined data from time point 1 of all 11 pathologists). Compared to category 1 (none to mild) as a reference, the hazard ratio of category 2 (moderate) is 5.0 (95% CI: 3.5 – 7.0,  $p < 0.001$ ) and for category 3 (severe) is 23.6 (95% CI: 16.1 – 34.2,  $p < 0.001$ ). **D)** Karyomegaly estimates (combined data from time point 1 of all 11 pathologists). The hazard ratio is 7.6 (95% CI: 5.7 – 10.1,  $p < 0.001$ ).

### Rater reproducibility

Inter-rater reproducibility for time point 1 was slight to fair for estimates of three-tier anisokaryosis ( $k = 0.187$ ) and karyomegaly ( $k = 0.226$ ) and good for measurements of mean nuclear area (ICC = 0.637, 95%CI: 0.482 – 0.750), SD of nuclear area (ICC = 0.654; 95%CI: 0.577 – 0.730) and maximum nuclear area (ICC = 0.683, 95%CI: 0.603 – 0.756). Intra-rater reproducibility between time points 1 and 2 was moderate for estimates of three-tier anisokaryosis ( $k = 0.60$ , 95%CI: 0.55 – 0.65) and karyomegaly ( $k = 0.51$ ; 95%CI: 0.44 – 0.58). The SD of the nuclear area corresponding to the different anisokaryosis category assigned by the individual pathologists is illustrated in Fig. 6. The figure shows that the predefined thresholds between the three anisokaryosis categories are differently interpreted by the pathologists.



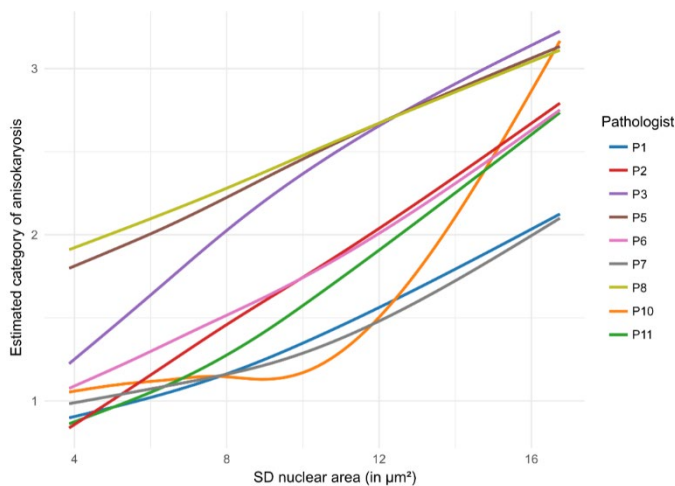


**Figure 6.** Illustration of the increase in the average three-tier anisokaryosis estimate depending on the algorithmic standard deviation (SD) of the nuclear area for each pathologist (curves determined by linear regression). The curves show which anisokaryosis category was likely assigned by the corresponding pathologist to a case depending on the SD of nuclear area measured. Curves were smoothed using a spline regression.

### Intra-tumoral Heterogeneity

Some variability in the measurements between the 3-5 ROI was noted for the different algorithmic morphometric parameters (Supplemental Table S17; Supplemental Fig. S14). Regarding the prognostic classification of SD of the nuclear area measurements based on threshold 1, 39/96 cases (41%) had divergent (low and high) measurements between the individual ROI (Table 3). However, the overall test performance (determined by the AUC) only increased mildly with the number of ROI used for statistical analysis, except for SD of eccentricity (Supplemental Figure S15).

Tumor heterogeneity as a prognostic test had high AUC value (Supplemental Table S18), which was, however, slightly lower than that for the mean of all ROI combined. For the morphometric parameter of SD of nuclear area, the SD between the different ROI had an AUC of 0.790 (95% CI: 0.632 – 0.947), and the proportion of hotspot ROI (above threshold 1 =  $9.0 \mu\text{m}^2$ ) had an AUC of 0.890 (95% CI: 0.780 – 1.00). With a higher proportion of hotspot ROI, the death probability increases (Table 3) and grouping cases with 0 – 20% vs.  $\geq 40\%$  hotspot ROI resulted in a sensitivity of 92.3% and specificity of 78.3%.

**Table 3.** Distribution of the outcome cases based on the proportion of hotspot regions of interest (ROI, classified by threshold 1) according to the standard deviation of nuclear area measurements (fully automated morphometry) <sup>a</sup> comparing cases with tumor-related mortality (TRM) to other cases without TRM. For each case 3 (N = 1), 4 (N = 4) or 5 (N = 91) ROI were analyzed.

Outcome	Proportion of hotspot ROI						
	0/3-5 (0%)	1/5 (20%)	2/5 (40%)	2/4 (50%)	3/5 (60%)	4/5 (80%)	5/5 (100%)
TRM	1	0	3	0	0	2	7
Other	47	18	6	1	6	3	2
Death probability	2%	0%	33%	0%	0%	40%	78%

<sup>a</sup> calculated by the number of ROI with a measurement above threshold 1 (9.0  $\mu\text{m}^2$ ) divided by the number of evaluated ROI.

## Discussion

The results of this study highlight the limitations of estimating nuclear characteristics of tumor cells as part of prognostic histologic evaluation, particularly with regard to rater reproducibility. Nuclear morphometry has several advantages over categorical evaluation of nuclear features; however, large numbers of cells cannot be measured by pathologists in a routine diagnostic setting. Our proposed automated nuclear morphometry approach is able to overcome these limitations while having a high prognostic value and practicability that allows integration into routine diagnostic workflow of laboratories that use digital microscopy.

Identification of nuclei and their outlines is generally a straightforward task for pathologists and algorithms. However, in heavily granulated ccMCT, nuclear membranes can be obscured and difficult to accurately outline. We therefore evaluated the measurement accuracy between algorithmic and manual morphometry. Compared to the ground truth, manual morphometry of 12 nuclei resulted in an overestimation of nuclear size, suggesting that pathologists had a tendency to oversample larger cells within the ROI. In contrast, the algorithm sampled most nuclei in the ROIs (no sampling bias) and is able to accurately segment mast cell nuclei, resulting in a smaller error for nuclear size measurements. Under-segmentation (algorithmic division of the image into too few segments, i.e. nuclei, leading to the interpretation of excessively large nuclei) is a potential problem for measuring karyomegalic cells; however, this was not commonly observed in the evaluated ccMCT cases. This can be explained by the lack of close cell contact between the neoplastic round cells and the moderate amount of cytoplasm that separates the neighboring nuclei. Potential sources of segmentation errors may be thick tissue sections, resulting in overlapping nuclei, or domain shift, resulting from different WSI scanners,<sup>3</sup> and the impact on morphometry should be explored in more detail by future studies. A drop of performance can also be expected when algorithms are applied to different tumor types.<sup>4</sup> Based on the frequency and extent of error in nuclear segmentation, different degrees of human-machine interaction (computer-assisted vs. fully automated prognosis) may be recommended to reduce errors during case evaluation.<sup>30</sup> In this study we did not apply any human-

machine interaction; however, we suggest that the model's segmentation mask should be verified visually by a trained pathologist if algorithmic morphometry is applied for routine diagnostic service.

Two-dimensional morphometric measurements were employed in the present study; however, other studies have used stereological estimates of nuclear volume (three-dimensional).<sup>13,39</sup> The rationale for estimating nuclear volume is that the measured area of the nucleus (a three-dimensional structure) in two-dimensional tissue sections is influenced by the position and orientation of the nucleus to the plane of section.<sup>11,13</sup> The incorrect assumption of orderly positioning and orientation of the nuclei along the plane of section introduces bias, such as the increased chance of evaluating larger nuclei more frequently.<sup>11</sup> While we acknowledge that our measurements may not perfectly correlate with 3D nuclear characteristics, we assume that our measurements follow statistical principles that allow calculation of the probability density function. We argue that random intercept measurements of approximately 75<sup>13</sup> or 166 ( $\pm 69$  SD)<sup>39</sup> nuclei is not much more representative than morphometry from accurate area measurements of all tumor cells (>1,000) in 5 random (with respect to nuclear characteristics) tumor regions. The benefit of 2D morphometry is that different parameters (mean, SD of nuclear area, 90<sup>th</sup> percentile etc.) of size and shape can be evaluated, while the stereologic approach is restricted to the mean volume. A direct comparison of the prognostic value of two- and three-dimensional-based methods may be an interesting subject for future studies.

All nuclear size parameters had good prognostic value (comparable with the mitotic count), while algorithmic morphometry predicted outcome a little bit better than manual morphometry on average. The prognostic ability of manual morphometry is impressive considering that this test was restricted to 12 representative nuclei, while algorithmic morphometry measured >1,000 nuclei in most cases. Our findings stand in contrast to the conclusions of Casanova et al.,<sup>13</sup> who found limited prognostic value of the volume-weighted mean nuclear volume (three-dimensional morphometry). While most size measurements had a very similar prognostic relevance, the parameters 90<sup>th</sup> percentile / median (approximating the 2011 karyomegaly definition<sup>23</sup>) was not particularly relevant in this study population due to the high correlation between the 90<sup>th</sup> percentile and median, which reduced the effect size of the quotient. Defining karyomegaly through the proportion of tumor cells with enlarged nuclei above a specific nuclear area (such as  $\geq 38 \mu\text{m}^2$ ) seems to be more appropriate; however, it is impractical for evaluations using traditional light microscopy. Of note, the manual measurement of one of the largest nuclei in the image (maximum measurement by pathologists), reflecting the presence or absence of a single karyomegalic cell, had surprisingly high prognostic value and may be a very practical prognostic test. Nuclear morphometry may represent a useful alternative to karyomegaly estimates for use in the 2011 grading system,<sup>23</sup> taking into account that the laboratory uses digital microscopy. Validation of our findings are needed in larger study populations. Another topic for future research is to combine different nuclear characteristics, such as nuclear size, shape, orientation, and spatial distribution.<sup>1,24</sup> In our study, algorithmic shape assessments had a markedly lower prognostic relevance than nuclear size parameters; however, it was beyond the scope of this study to evaluate whether nuclear shape assessments can add prognostic information when combined with nuclear size parameters. Further studies are needed to evaluate the measurement accuracy and prognostic relevance of the different morphometric parameters of automated morphometry for further tumor types.

The results of this study show low inter-rater reproducibility for anisokaryosis estimates in ccMCT. Given the wide variations in sensitivity and specificity when comparing individual pathologist's estimates, this parameter has different prognostic value between pathologists. Two issues that can contribute to low inter-rater reproducibility are: 1) distinct anisokaryosis / nuclear pleomorphism categories are difficult to precisely define and 2) the defined thresholds between the categories are interpreted differently by individual pathologists. A vague definition of the categories (i.e. mild, moderate, severe or similar) is common in current literature;<sup>15,33</sup> thus, we decided to use a similar approach for the three-tier anisokaryosis method. Other studies provide a more specific definition for the anisokaryosis categories with percentage of affected cells and/or degree (X-fold) of nuclear size variation,<sup>23,28</sup> as for the karyomegaly definition used in this study. Regardless of the use of a vague or more specific definition, study participants had difficulty applying the categories in the same manner. Further studies are needed to evaluate methods that improve reproducibility, such as pictorial illustrations of each category or reference sizes within the image based on a scale overlay (digital microscopy) or non-tumor cell within the image (light microscopy), similar to that used for the lymphoma subtype classification.<sup>42</sup> Of note, average neoplastic mast cells in the tumor section seem to be a less ideal reference size, as aggressive tumors not only have a higher variation in nuclear size but also a higher mean/median area.

Low reproducibility of pathologists' estimates is the main motivation for morphometry<sup>13,39</sup> and the development of the different algorithmic approaches (see introduction). Using one algorithm will result in 100% reproducibility;<sup>9</sup> however, the reproducibility between different segmentation models (based on different network architectures and/or training/validation data) that may be applied in different laboratories needs to be evaluated. Manual morphometry has been shown to have high reproducibility,<sup>13</sup> but it is impractical to measure a larger number of cells for routine diagnostic pathology. In our study, we limited the number of cells to 12 with the intention of creating a fairly practical quantitative test. Despite improved reproducibility as compared to estimates, significant differences between pathologists were still noted, suggesting that 12 selected nuclei are not representative enough for each case. Interestingly, the maximum area of manual morphometry had the highest inter-rater reproducibility in this study, while also having a good prognostic value. Measuring just one of the largest neoplastic nuclei in the tumor section would improve the feasibility of applying morphometry and should be evaluated as a prognostic factor in future studies. However, due to intra-tumoral heterogeneity, reproducibility may be reduced when this task is performed on WSI and not restricted to a few preselected tumor regions.

Tumor heterogeneity is interesting regarding sampling strategies of tumor regions and understanding tumor biology. The use of a deep learning-based algorithm allowed us to analyze several ROI and thus enabled intra-tumoral comparison of morphometric measurements in ccMCT for the first time. Although we observed variability of the morphometric measurements between the different tumor regions, the number of ROI used for prognostic evaluation generally had a minor effect on the determined AUC values. While analysis of a single ROI provided a satisfactory prognostic interpretation of the case, a higher number of ROI might be slightly beneficial. Of note, the maximum value of the analyzed ROI per case did not result in a higher discriminative ability of patient survival than the average of all ROI. However, as we had selected the representative tumor regions without attention to nuclear features and restricted the analysis to a few ROI, it remains unknown whether areas with the highest

morphometric values in the tumor section would be favorable for prognostic assessment of the case.

It is very intriguing that intra-tumoral heterogeneity of morphometry itself had a moderate to good discriminative ability for patient survival, even though the heterogeneity measurement was restricted to 5 tumor regions. It would be interesting to explore the distribution of nuclear parameters throughout the entire tumor sections, as has been previously done for nuclear morphometry in human tumors <sup>1</sup> or for the mitotic count in ccMCT.<sup>6,7</sup> Particularly the prognostic test “proportion of hotspot ROI” would probably benefit from a more comprehensive analysis of the entire tumor section. These fully automated nuclear morphometry algorithms have great potential for employing intra-tumoral heterogeneity as a routine prognostic test.

## Conclusion

Poor inter-reproducibility of anisokaryosis estimates hinders meaningful application of this test for routine tumor prognostication. An alternative to estimation is nuclear morphometry, the advantages of which include high reproducibility and the capability of determining meaningful prognostic thresholds based on the association with patient outcome. While manual measurements of a larger number of cells is impractical for routine application, we have shown that assessment of a few (12) tumor nuclei provides meaningful prognostic information; however, results in insufficient inter-rater consistency. We are proposing a deep learning-based algorithm that is capable of analyzing thousands of cells within seconds at low computational costs. This study demonstrated a high measurement accuracy and high prognostic value of fully automated nuclear morphometry for ccMCT. In this study population of 95 ccMCT cases, morphometric parameters evaluating the nuclear area (such as the standard deviation or 90<sup>th</sup> percentile) were particularly prognostically relevant. The results of this study encourage application of automated nuclear morphometry for routine tumor evaluation in laboratories with established digital workflows. A more thorough investigation of tumor heterogeneity and its prognostic value is warranted based on our preliminary findings with a relatively low number of tumor regions.

## Acknowledgement

Parts of this research was conducted for the diploma project of Eda Parlak using a preliminary version of the DL-based algorithm.

## Declaration of conflict of interest

The author(s) declared no potential conflicts of interest with respect to the research, authorship, and/or publication of this article.

## Funding

The author(s) received no financial support for the research, authorship, and/or publication of this article.

## Authors' Contributions

CAB, AH, EP, TAD, and AB designed the experiments; MK, CAB, TAD and RK contributed histological sections; MK provided outcome information; EP developed the ground truth dataset; AH developed the algorithm; MA, SMW, and JS contributed to algorithm development; CAB and JG organized the pathologist experiment; TAD, CAA, PB, MJD, AFB, AK, KJ, RK, SM, BR, and FYS participated as study pathologists; CAB performed mitotic counts; CAB, AH, AB, and EP performed data analysis; the manuscript was written by CAB and AH with contributions by all authors.

## References

1. Alsubaie NM, Snead D, Rajpoot NM. Tumour nuclear morphometrics predict survival in lung adenocarcinoma. *IEEE Access*. 2021;9: 12322-12331.
2. Aubreville M, Bertram C, Klopfleisch R, Maier A: Sliderunner: A tool for massive cell annotations in whole slide images. *In: Bildverarbeitung für die Medizin 2018: Algorithmen-Systeme-Anwendungen. Proceedings des Workshops vom 11. bis 13. März 2018 in Erlangen*, pp. 309-314. Springer, 2018
3. Aubreville M, Stathonikos N, Bertram CA, et al. Mitosis domain generalization in histopathology images - The MIDOG challenge. *Med Image Anal*. 2023;84: 102699. 10.1016/j.media.2022.102699
4. Aubreville M, Wilm F, Stathonikos N, et al. A comprehensive multi-domain dataset for mitotic figure detection. *Sci Data*. 2023;10: 484. 10.1038/s41597-023-02327-4
5. Berlato D, Bulman-Fleming J, Clifford CA, et al. Value, limitations, and recommendations for grading of canine cutaneous mast cell tumors: a consensus of the oncology-pathology working group. *Vet Pathol*. 2021;58: 858-863. doi: 10.1177/03009858211009785
6. Bertram CA, Aubreville M, Donovan TA, et al. Computer-assisted mitotic count using a deep learning-based algorithm improves interobserver reproducibility and accuracy. *Vet Pathol*. 2022;59: 211-226. 10.1177/03009858211067478
7. Bertram CA, Aubreville M, Gurtner C, et al. Computerized Calculation of Mitotic Count Distribution in Canine Cutaneous Mast Cell Tumor Sections: Mitotic Count Is Area Dependent. *Vet Pathol*. 2020;57: 214-226. 10.1177/0300985819890686
8. Bertram CA, Donovan TA, Bartel A. Systematic Review of Methods and Prognostic Value of Mitotic Activity. Part 2: Canine Tumors. *arXiv preprint arXiv:230519667*. 2023.
9. Bertram CA, Klopfleisch R. The Pathologist 2.0: An Update on Digital Pathology in Veterinary Medicine. *Vet Pathol*. 2017;54: 756-766. 10.1177/0300985817709888
10. Brocks BAW, Bertram CA, Bartel A, et al. Internal Tandem Duplication of Exon 8 of c-kit Is Associated With Longer Total Survival in Canine Cutaneous Mast Cell Tumors. *Vet Pathol*. 2021;58: 315-324. 10.1177/0300985820973463
11. Brown DL. Practical Stereology Applications for the Pathologist. *Vet Pathol*. 2017;54: 358-368. 10.1177/0300985817695781
12. Camus MS, Priest HL, Koehler JW, et al. Cytologic Criteria for Mast Cell Tumor Grading in Dogs With Evaluation of Clinical Outcome. *Vet Pathol*. 2016;53: 1117-1123. doi: 10.1177/0300985816638721
13. Casanova M, Branco S, Veiga IB, Barros A, Faisca P. Stereology in Grading and Prognosis of Canine Cutaneous Mast Cell Tumors. *Vet Pathol*. 2021;58: 483-490. 10.1177/0300985820985138
14. Chuang WY, Yu WH, Lee YC, et al. Deep Learning-Based Nuclear Morphometry Reveals an Independent Prognostic Factor in Mantle Cell Lymphoma. *Am J Pathol*. 2022;192: 1763-1778. 10.1016/j.ajpath.2022.08.006

15. Dagher E, Abadie J, Loussouarn D, Campone M, Nguyen F. Feline Invasive Mammary Carcinomas: Prognostic Value of Histological Grading. *Vet Pathol.* 2019;56: 660-670. 10.1177/0300985819846870
16. Dettwiler M, Mauldin EA, Jastrebski S, Gillette D, Stefanovski D, Durham AC. Prognostic clinical and histopathological features of canine cutaneous epitheliotropic T-cell lymphoma. *Vet Pathol.* 2023;60: 162-171. 10.1177/03009858221140818
17. Donovan TA, Moore FM, Bertram CA, et al. Mitotic Figures-Normal, Atypical, and Imposters: A Guide to Identification. *Vet Pathol.* 2021;58: 243-257. 10.1177/0300985820980049
18. Falcon W: PyTorch Lightning. GitHub. Note: <https://github.com/PyTorchLightning/pytorch-lightning>,. 2019
19. Hallgren KA. Computing Inter-Rater Reliability for Observational Data: An Overview and Tutorial. *Tutor Quant Methods Psychol.* 2012;8: 23-34. 10.20982/tqmp.08.1.p023
20. Horta RS, Lavallo GE, Monteiro LN, Souza MCC, Cassali GD, Araújo RB. Assessment of Canine Mast Cell Tumor Mortality Risk Based on Clinical, Histologic, Immunohistochemical, and Molecular Features. *Vet Pathol.* 2018;55: 212-223. 10.1177/0300985817747325
21. Iakubovskii P. Segmentation Models Pytorch. Note: [https://github.com/qubvel/segmentation\\_models.pytorch](https://github.com/qubvel/segmentation_models.pytorch). 2019.
22. Kiupel M, Camus M. Diagnosis and Prognosis of Canine Cutaneous Mast Cell Tumors. *Vet Clin North Am Small Anim Pract.* 2019;49: 819-836. 10.1016/j.cvsm.2019.04.002
23. Kiupel M, Webster JD, Bailey KL, et al. Proposal of a 2-tier histologic grading system for canine cutaneous mast cell tumors to more accurately predict biological behavior. *Vet Pathol.* 2011;48: 147-155. 10.1177/0300985810386469
24. Lu C, Romo-Bucheli D, Wang X, et al. Nuclear shape and orientation features from H&E images predict survival in early-stage estrogen receptor-positive breast cancers. *Lab Invest.* 2018;98: 1438-1448. 10.1038/s41374-018-0095-7
25. Maiolino P, Cataldi M, Paciello O, Restucci B, De Vico G. Nucleomorphometric analysis of canine cutaneous mast cell tumours. *J Comp Pathol.* 2005;133: 209-211. 10.1016/j.jcpa.2005.02.002
26. Marzahl C, Aubreville M, Bertram CA, et al. EXACT: a collaboration toolset for algorithm-aided annotation of images with annotation version control. *Sci Rep.* 2021;11: 4343. 10.1038/s41598-021-83827-4
27. Mathew T, Johnpaul C, Ajith B, Kini JR, Rajan J. A deep learning based classifier framework for automated nuclear atypia scoring of breast carcinoma. *Engineering Applications of Artificial Intelligence.* 2023;120: 105949.
28. McNiel EA, Ogilvie GK, Powers BE, Hutchison JM, Salman MD, Withrow SJ. Evaluation of prognostic factors for dogs with primary lung tumors: 67 cases (1985-1992). *J Am Vet Med Assoc.* 1997;211: 1422-1427.
29. Mercan C, Balkenhol M, Salgado R, et al. Deep learning for fully-automated nuclear pleomorphism scoring in breast cancer. *NPJ Breast Cancer.* 2022;8: 120. 10.1038/s41523-022-00488-w
30. Meuten DJ, Moore FM, Donovan TA, et al. International Guidelines for Veterinary Tumor Pathology: A Call to Action. *Vet Pathol.* 2021;58: 766-794. 10.1177/03009858211013712
31. Mills SW, Musil KM, Davies JL, et al. Prognostic value of histologic grading for feline mammary carcinoma: a retrospective survival analysis. *Vet Pathol.* 2015;52: 238-249. 10.1177/0300985814543198

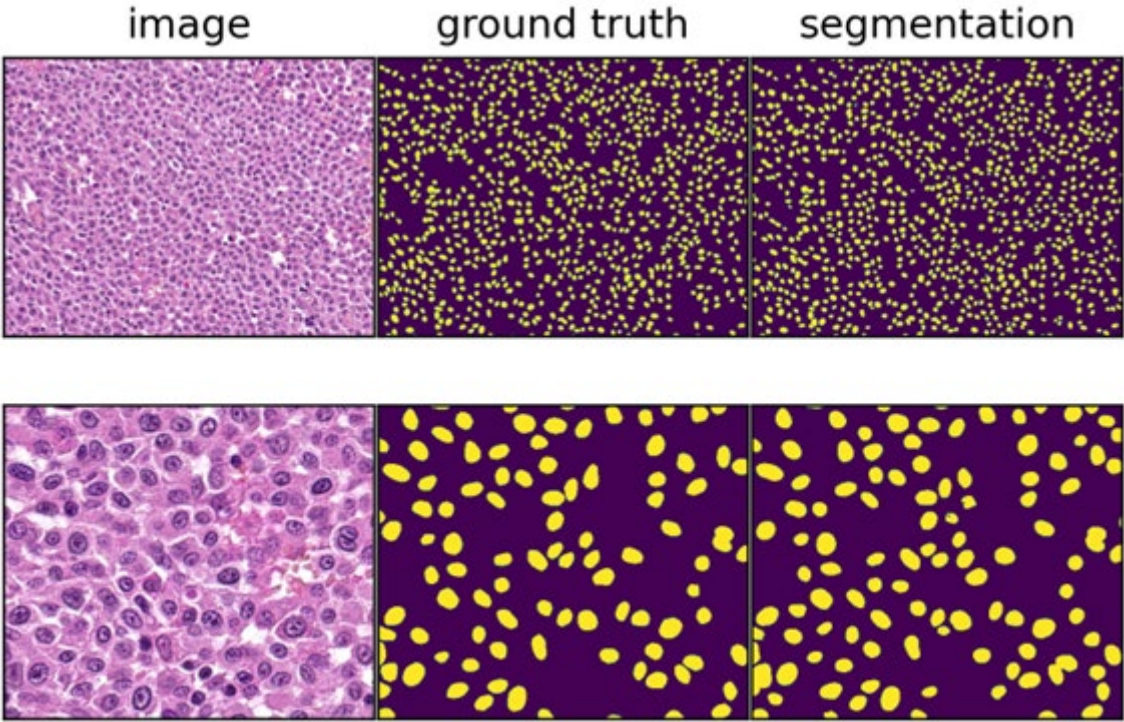
32. Patnaik AK, Ehler WJ, MacEwen EG. Canine cutaneous mast cell tumor: morphologic grading and survival time in 83 dogs. *Vet Pathol.* 1984;21: 469-474. 10.1177/030098588402100503
33. Peña L, De Andrés PJ, Clemente M, Cuesta P, Pérez-Alenza MD. Prognostic value of histological grading in noninflammatory canine mammary carcinomas in a prospective study with two-year follow-up: relationship with clinical and histological characteristics. *Vet Pathol.* 2013;50: 94-105. 10.1177/0300985812447830
34. Pradel J, Berlato D, Dobromylskyj M, Rasotto R. Prognostic significance of histopathology in canine anal sac gland adenocarcinomas: Preliminary results in a retrospective study of 39 cases. *Vet Comp Oncol.* 2018;16: 518-528. 10.1111/vco.12410
35. Radosavovic I, Kosaraju RP, Girshick R, He K, Dollár P: Designing network design spaces. *In: Proceedings of the IEEE/CVF conference on computer vision and pattern recognition*, pp. 10428-10436. 2020
36. Romansik EM, Reilly CM, Kass PH, Moore PF, London CA. Mitotic index is predictive for survival for canine cutaneous mast cell tumors. *Vet Pathol.* 2007;44: 335-341. doi: 10.1354/vp.44-3-335
37. Sabattini S, Bettini G. Grading Cutaneous Mast Cell Tumors in Cats. *Vet Pathol.* 2019;56: 43-49. 10.1177/0300985818800028
38. Santos M, Correia-Gomes C, Santos A, de Matos A, Dias-Pereira P, Lopes C. Interobserver Reproducibility of Histological Grading of Canine Simple Mammary Carcinomas. *J Comp Pathol.* 2015;153: 22-27. 10.1016/j.jcpa.2015.04.005
39. Santos M, Correia-Gomes C, Santos A, et al. Nuclear pleomorphism: role in grading and prognosis of canine mammary carcinomas. *Vet J.* 2014;200: 426-433. 10.1016/j.tvjl.2014.03.019
40. Simoes JP, Schoning P, Butine M. Prognosis of canine mast cell tumors: a comparison of three methods. *Vet Pathol.* 1994;31: 637-647. 10.1177/030098589403100602
41. Strefezzi Rde F, Xavier JG, Kleeb SR, Catão-Dias JL. Nuclear morphometry in cytopathology: a prognostic indicator for canine cutaneous mast cell tumors. *J Vet Diagn Invest.* 2009;21: 821-825. 10.1177/104063870902100608
42. Valli VE, San Myint M, Barthel A, et al. Classification of canine malignant lymphomas according to the World Health Organization criteria. *Vet Pathol.* 2011;48: 198-211. 10.1177/0300985810379428
43. van der Walt S, Schönberger JL, Nunez-Iglesias J, et al. scikit-image: image processing in Python. *PeerJ.* 2014;2: e453. 10.7717/peerj.453
44. Veta M, Kornegoor R, Huisman A, et al. Prognostic value of automatically extracted nuclear morphometric features in whole slide images of male breast cancer. *Mod Pathol.* 2012;25: 1559-1565. 10.1038/modpathol.2012.126
45. Zhou Z, Siddiquee MMR, Tajbakhsh N, Liang J. UNet++: A Nested U-Net Architecture for Medical Image Segmentation. *Deep Learn Med Image Anal Multimodal Learn Clin Decis Support (2018).* 2018;11045: 3-11. 10.1007/978-3-030-00889-5\_1



Supplemental Material

Method Accuracy

DL- based Algorithm (Automated Nuclear Morphometry)

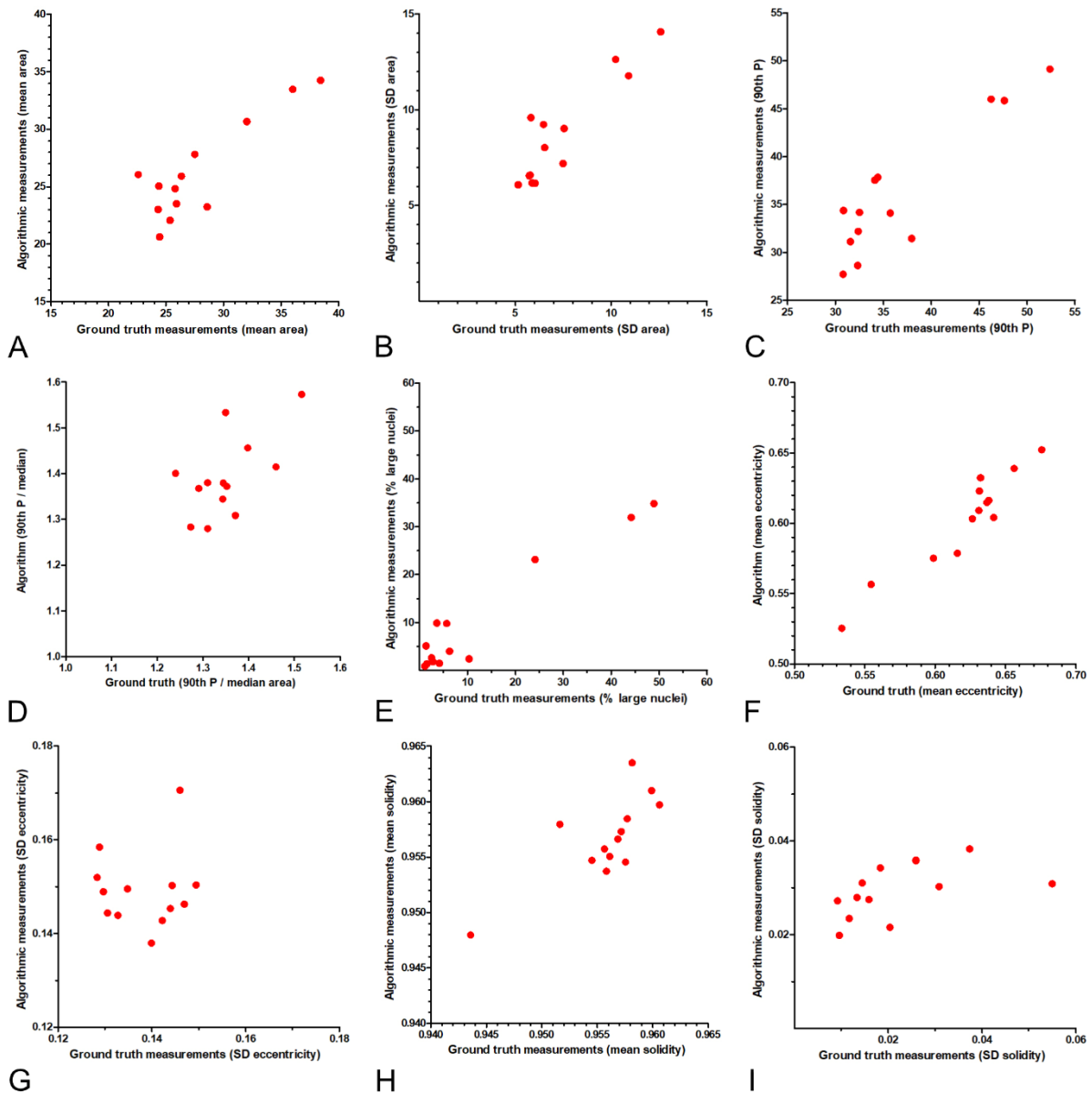


**Supplemental Figure S1.** Comparison of the ground truth and the segmentation mask derived from the deep learning-based model. The yellow areas represent the segmented mast cell tumor nuclei.

**Supplemental Table S1.** Root mean squared error (RMSE) for the different morphometric parameters comparing the measurements of the deep learning-based algorithm to the ground truth measurements for the 13 cases of the test dataset.

Feature	Morphometric parameter	Root mean squared error (RMSE)	Value range ground truth measurement	RMSE to range ratio (coefficient of variation)
Size (area in $\mu\text{m}^2$ )	Mean	2.78 $\mu\text{m}^2$	22.59 – 38.43 $\mu\text{m}^2$	17.6%
	Median	2.54 $\mu\text{m}^2$	22.51 – 37.47 $\mu\text{m}^2$	17.0%
	SD	1.69 $\mu\text{m}^2$	5.15 – 12.58 $\mu\text{m}^2$	22.8%
	90 <sup>th</sup> percentile (P)	3.04 $\mu\text{m}^2$	30.81 – 52.38 $\mu\text{m}^2$	14.1%
	90 <sup>th</sup> P / median	0.081	1.240 – 1.516	29.4%
	Mean of the largest 10%	4.83 $\mu\text{m}^2$	34.18 – 63.86 $\mu\text{m}^2$	16.3%
	Percentage large nuclei (>37.8 $\mu\text{m}^2$ )	6.17%	1.16 – 48.91%	12.9%
	Percentage large nuclei (>50.3 $\mu\text{m}^2$ )	1.37%	0 – 11.95%	11.5%
	Skewness	0.802	-0.583 – 1.617	36.4%
Shape	Mean eccentricity	0.022	0.533 – 0.676	15.5%
	SD of eccentricity	0.015	0.128 – 0.149	71.8%
	Skewness eccentricity	0.285	-1.513 – -0.042	19.4%
	Mean solidity	0.003	0.943 – 0.960	16.7%
	SD of solidity	0.013	0.009 – 0.055	28.5%
	Percentage of nuclei with indentation (solidity <0.913)	3.54%	0.19 - 7.55%	48.2%
	Skewness solidity	3.69	-9.24 – -1.30	46.5%

SD, standard deviation

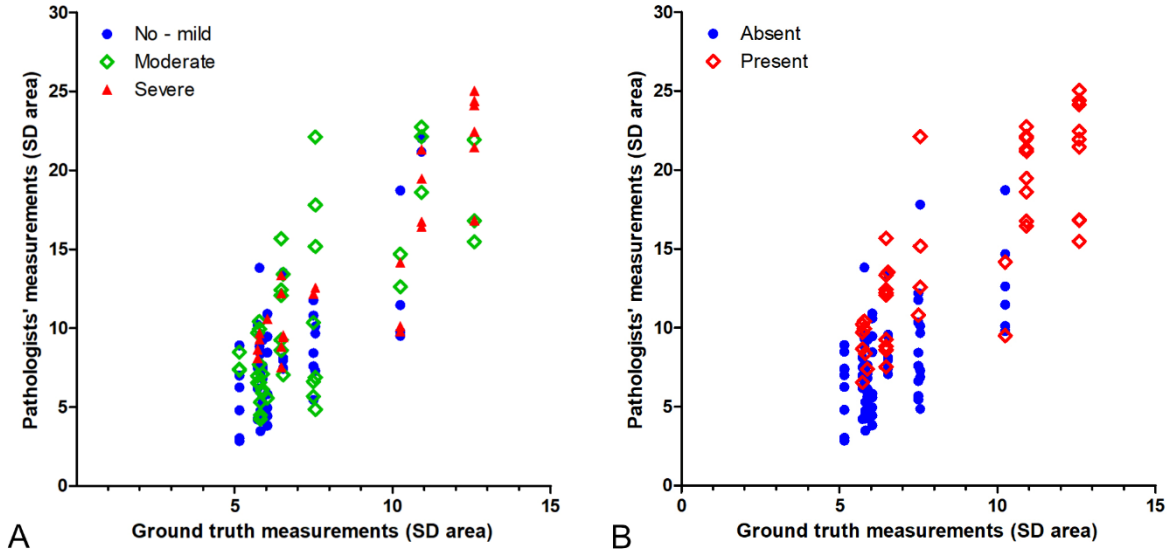


**Supplemental Figure S2.** Scatter plot of the different morphometric parameters comparing the algorithmic measurements with the ground truth measurements for the 13 cases of the test dataset. **A)** mean nuclear area in  $\mu\text{m}^2$ , **B)** standard deviation (SD) of nuclear area in  $\mu\text{m}^2$ , **C)** 90% percentile (90%P) of nuclear area in  $\mu\text{m}^2$ , **D)** 90%P / median nuclear area, **E)** percentage (%) of large nuclei with an area  $>37.8 \mu\text{m}^2$ , **F)** Mean eccentricity **G)** SD of eccentricity, **H)** Mean solidity, **I)** SD of solidity

**Pathologists' Measurements (Manual Nuclear Morphometry)**

**Supplemental Table S2.** Root mean squared error (RMSE) for the standard deviation of the manual nuclear area measurements of the 9 individual pathologists compared to the ground truth measurements (standard deviation of the area) for the 13 cases of the test dataset.

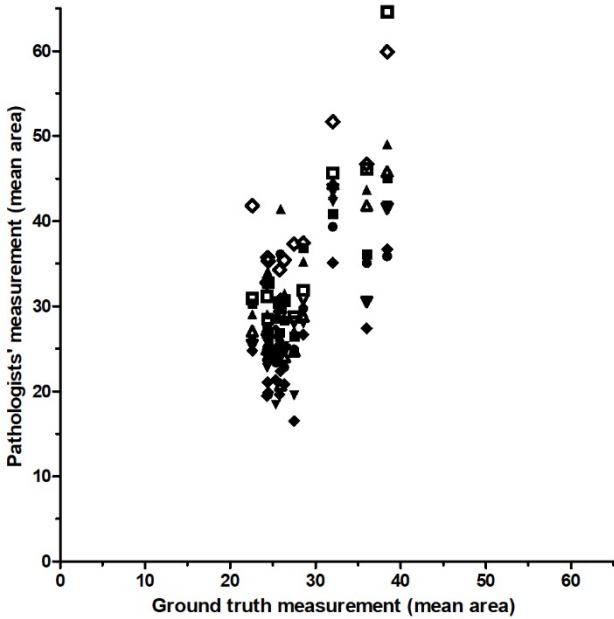
Pathologist	Root squared error (RMSE)	mean error	Value ground measurement	range truth	RMSE to range ratio (coefficient of variation)
Pathologist 1	3.79 $\mu\text{m}^2$		5.15 – 12.58 $\mu\text{m}^2$		51.0%
Pathologist 2	5.32 $\mu\text{m}^2$		5.15 – 12.58 $\mu\text{m}^2$		71.7%
Pathologist 3	3.93 $\mu\text{m}^2$		5.15 – 12.58 $\mu\text{m}^2$		52.8%
Pathologist 5	4.41 $\mu\text{m}^2$		5.15 – 12.58 $\mu\text{m}^2$		59.4%
Pathologist 6	7.53 $\mu\text{m}^2$		5.15 – 12.58 $\mu\text{m}^2$		101.3%
Pathologist 7	4.83 $\mu\text{m}^2$		5.15 – 12.58 $\mu\text{m}^2$		65.1%
Pathologist 8	4.05 $\mu\text{m}^2$		5.15 – 12.58 $\mu\text{m}^2$		54.5%
Pathologist 10	3.97 $\mu\text{m}^2$		5.15 – 12.58 $\mu\text{m}^2$		53.5%
Pathologist 11	5.65 $\mu\text{m}^2$		5.15 – 12.58 $\mu\text{m}^2$		76.0%
Mean measurement	4.18 $\mu\text{m}^2$		5.15 – 12.58 $\mu\text{m}^2$		56.3%



**Supplemental Figure S3.** Scatter plot of the standard deviation (SD) of nuclear area comparing the pathologists' (N = 9) measurements with the ground truth measurements for the 13 cases of the test subset of the ground truth dataset. **A)** Each datapoint is classified by the estimated degree of three-tier anisokaryosis assigned by the same pathologist. **B)** Each datapoint is classified by the estimated degree of two-tier karyomegaly assigned by the same pathologist.

**Supplemental Table S3.** Root mean squared error (RMSE) for the mean of the manual nuclear area measurements of the individual pathologists compared to the ground truth measurements (mean area) for the 13 cases of the test dataset.

Pathologist	Root squared (RMSE)	mean error	Value ground measurement	range truth	RMSE to range ratio (coefficient of variation)
Pathologist 1	4.74		22.59 – 38.43 $\mu\text{m}^2$		29.9%
Pathologist 2	8.04		22.59 – 38.43 $\mu\text{m}^2$		50.8%
Pathologist 3	4.67		22.59 – 38.43 $\mu\text{m}^2$		29,5%
Pathologist 5	5.33		22.59 – 38.43 $\mu\text{m}^2$		33.7%
Pathologist 6	4.16		22.59 – 38.43 $\mu\text{m}^2$		26.2%
Pathologist 7	9.77		22.59 – 38.43 $\mu\text{m}^2$		61.7%
Pathologist 8	5.01		22.59 – 38.43 $\mu\text{m}^2$		31.6%
Pathologist 10	4.05		22.59 – 38.43 $\mu\text{m}^2$		25.6%
Pathologist 11	12.40		22.59 – 38.43 $\mu\text{m}^2$		78.3%
Mean measurements	5.38		22.59 – 38.43 $\mu\text{m}^2$		34.0%

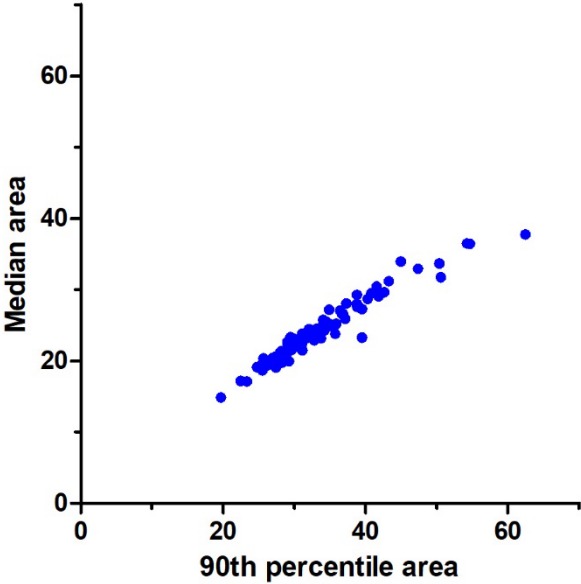


**Supplemental Figure S4.** Scatter plot of the mean nuclear area comparing the pathologists' (N = 9) measurements with the ground truth measurements for the 13 cases of the test subset of the ground truth dataset.

**Correlation of Morphometric Parameters**

**Table S4.** Correlation coefficients (Pearson method) for comparison of the individual area parameters measured by algorithmic nuclear morphometry in the 96 outcome cases. The cells in the table are color coded with correlation coefficients of 0 being white and 1 being dark blue.

	Mean	Median	SD	90%P	90 <sup>th</sup> P / median	Mean largest 10%	% above 37.8 $\mu\text{m}^2$	% above 50.3 $\mu\text{m}^2$
Mean	1							
Median	0,996	1						
SD	0,936	0,910	1					
90 <sup>th</sup> percentile (P)	0,985	0,970	0,975	1				
90 <sup>th</sup> P / median	0,508	0,446	0,750	0,640	1			
Mean of the largest 10%	0,974	0,955	0,988	0,943	0,665	1		
Percent of cells above 37.8 $\mu\text{m}^2$	0,930	0,911	0,925	0,948	0,606	0,943	1	
Percent of cells above 50.3 $\mu\text{m}^2$	0,811	0,776	0,850	0,860	0,642	0,848	0,912	1



**Supplemental Figure S5.** Scatterplot comparing the 90<sup>th</sup> percentile and median nuclear area measurements (in  $\mu\text{m}^2$ ) of the 96 outcome cases measured by algorithmic nuclear morphometry. These two morphometric parameters have a Pearson correlation coefficient of 0.970.

## Prognostic Value

### Demographic information of the study population

Dogs of various breeds were included in this study: mixed-breed (N = 21), Labrador Retriever (N = 21), Boxer (N = 11), Golden Retriever (N = 10), Pug (N = 4), Basset Hound (N = 4), Boston Terrier (N = 3), Cocker Spaniel (N = 3), and other breeds (N = 19). These 96 dogs were spayed female (N = 51), castrated males (N = 33), intact females (N = 7) and intact males (N = 5). Their age was within following ranges: older than 10 years (N = 26), between 6 – 9 years (N = 40), between 3 – 5 years (N = 27), and younger than 2 years (N = 3). No dog received any therapy for the mast cell tumor besides excisional surgery with curative intent.

### Area Under the Curve

**Supplemental Table S5.** Area under the ROC curve (AUC) with 95% confidence intervals (95% CI) for the individual parameters of algorithmic nuclear morphometry regarding tumor-specific survival throughout the entire follow-up period. The mitotic count (benchmark) archived an AUC of 0.885 (95%CI: 0.765 - 1.00,  $p < 0.001$ ).

Morphometric feature	Morphometric parameter	AUC (95% CI)
Size (area in $\mu\text{m}^2$ )	Mean	0.921 (0.839 – 1.00) **
	Median	0.918 (0.832 – 1.00) **
	Standard deviation (SD)	0.943 (0.889 – 0.996) **
	90 <sup>th</sup> percentile (90 <sup>th</sup> P)	0.932 (0.862 – 1.00) **
	90 <sup>th</sup> P/ median	0.846 (0.728 – 0.964) **
	Mean of the largest 10% of the nuclei	0.932 (0.864 – 1.00) **
	Percentage of large nuclei (>37.8 $\mu\text{m}^2$ )	0.925 (0.849 – 1.00) **
	Percentage of large nuclei (>50.3 $\mu\text{m}^2$ )	0.909 (0.815 – 1.00) **
	Skewness	0.665 (0.510 – 0.819) *
Shape	Mean eccentricity	0.471 (0.325 – 0.617)
	SD of eccentricity	0.825 (0.728 – 0.921) **
	Skewness eccentricity	0.615 (0.468 – 0.762)
	1 - Mean solidity	0.553 (0.390 – 0.706)
	SD of solidity	0.761 (0.641 – 0.881) **
	Percentage of nuclei with indentation (solidity <0.913)	0.757 (0.631 - 0.883) **
	Percentage of nuclei with indentation (solidity <0.936)	0.691 (0.555 - 0.828) *
	Percentage of nuclei with indentation (solidity < 0.943)	0.640 (0.497 - 0.784)
	Skewness solidity	0.670 (0.519 – 0.821) *

\*  $p \leq 0.05$ ; \*\*  $p \leq 0.001$

**Supplemental Table S6.** Area under the ROC curve (AUC) with 95% confidence intervals (95% CI) for the individual parameters of algorithmic nuclear morphometry regarding tumor-specific survival at 12 months after surgery. Cases that had died within the first 12 months after surgery due to an ccMCT-unrelated cause (N = 6) were excluded for this analysis. The mitotic count (benchmark) archived an AUC of 0.890 (95% CI: 0.797 – 0.982; p < 0.001).

<b>Morphometric feature</b>	<b>Morphometric parameter</b>	<b>AUC (95% CI)</b>
Size (area in $\mu\text{m}^2$ )	Mean	0.884 (0.737 – 0.992) **
	Median	0.862 (0.731 – 0.992) **
	Standard deviation (SD)	0.886 (0.780 – 0.992) **
	90 <sup>th</sup> percentile (90 <sup>th</sup> P)	0.881 (0.769 – 0.994) **
	90 <sup>th</sup> P/ median	0.827 (0.690 – 0.965) **
	Mean of the largest 10% of the nuclei	0.873 (0.758 – 0.988) **
	Percentage of large nuclei (>37.8 $\mu\text{m}^2$ )	0.862 (0.729 – 0.995) **
	Percentage of large nuclei (>50.3 $\mu\text{m}^2$ )	0.808 (0.625 – 0.992) **
	Skewness	0.536 (0.354 – 0.718)
Shape	Mean eccentricity	0.495 (0.331 – 0.659)
	SD of eccentricity	0.750 (0.624 – 0.877) **
	Skewness eccentricity	0.589 (0.415 – 0.763)
	1 - Mean solidity	0.572 (0.400 – 0.743)
	SD of solidity	0.768 (0.661 – 0.874) **
	Percentage of nuclei with indentation (solidity <0.913)	0.741 (0.609 - 0.873) **
	Skewness solidity	0.624 (0.448 – 0.800)

\* p ≤ 0.05; \*\* p ≤ 0.001



**Supplemental Table S7.** Area under the ROC curve (AUC) with 95% confidence intervals (95% CI) for the individual parameters of algorithmic nuclear morphometry regarding overall mortality at 12 months after surgery (cases with death within the first 12 months after surgery regardless of cause compared to cases that survived for at least 12 months). The mitotic count (benchmark) archived an AUC of 0.744 (95% CI: 0.596 – 0.891, p = 0.001).

<b>Morphometric feature</b>	<b>Morphometric parameter</b>	<b>AUC (95% CI)</b>
Size (area in $\mu\text{m}^2$ )	Mean	0.730 (0.568 – 0.893) *
	Median	0.723 (0.558 – 0.888) *
	Standard deviation (SD)	0.766 (0.618 – 0.914) **
	90 <sup>th</sup> percentile (90 <sup>th</sup> P)	0.749 (0.593 – 0.906) *
	90 <sup>th</sup> P / median	0.696 (0.524 – 0.869) *
	Mean of the largest 10% of the nuclei	0.744 (0.590 – 0.897) *
	Percentage of large nuclei (>37.8 $\mu\text{m}^2$ )	0.755 (0.602 – 0.907) **
	Percentage of large nuclei (>50.3 $\mu\text{m}^2$ )	0.738 (0.590 – 0.887) *
	Skewness	0.524 (0.379 – 0.669)
Shape	Mean eccentricity	0.441 (0.272 – 0.610)
	SD of eccentricity	0.606 (0.452 – 0.760)
	Skewness eccentricity	0.630 (0.459 – 0.800)
	1 - Mean solidity	0.458 (0.401 – 0.719)
	SD of solidity	0.691 (0.558 – 0.825) *
	Percentage of nuclei with indentation (solidity <0.913)	0.700 (0.560 - 0.840) *
	Skewness solidity	0.610 (0.447 – 0.773)

\* p ≤ 0.05; \*\* p ≤ 0.001

**Supplemental Table S8.** Area under the ROC curve (AUC) with 95% confidence intervals (95% CI) for manual nuclear morphometry of the individual pathologists regarding tumor-specific survival throughout the entire follow-up period.

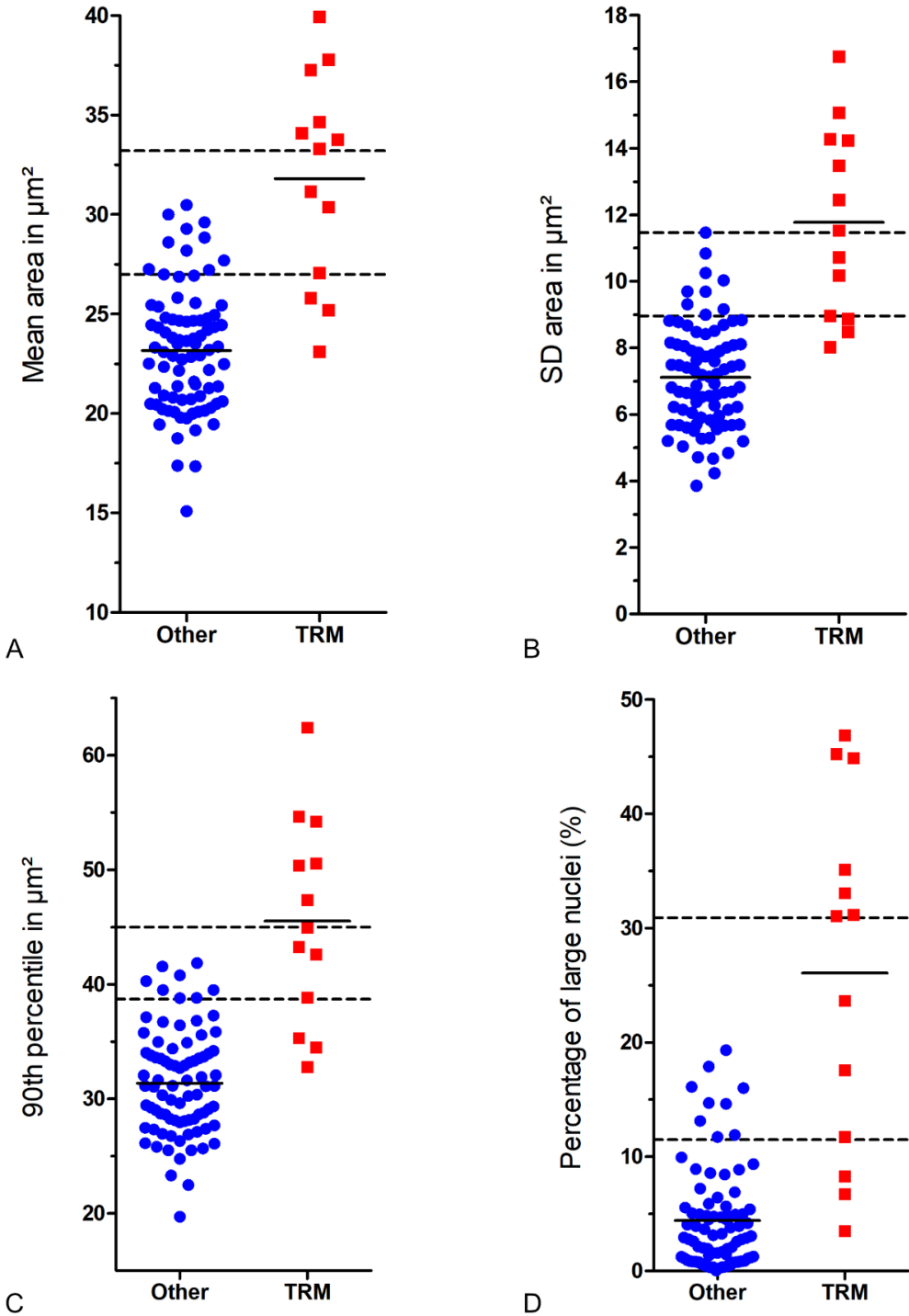
Path-ologist	AUC (95% CI)		
	Mean area	SD of area	Maximum area
P1	0.957 (0.917 – 0.998)	0.905 (0.842 – 0.969)	0.925 (0.870 – 0.980)
P2	0.898 (0.820 – 0.976)	0.852 (0.754 – 0.949)	0.898 (0.828 – 0.967)
P3	0.885 (0.771 – 0.999)	0.890 (0.781 – 0.999)	0.886 (0.755 – 1.00)
P5	0.883 (0.791 – 0.976)	0.823 (0.678 – 0.968)	0.841 (0.717 – 0.964)
P6	0.949 (0.902 – 0.997)	0.835 (0.741 – 0.929)	0.880 (0.806 – 0.953)
P7	0.912 (0.834 – 0.990)	0.960 (0.918 – 1.00)	0.956 (0.908 – 1.00)
P8	0.862 (0.747 – 0.979)	0.842 (0.720 – 0.963)	0.817 (0.699 – 0.935)
P10	0.878 (0.771 – 0.985)	0.834 (0.679 – 0.990)	0.839 (0.712 – 0.967)
P11	0.857 (0.758 – 0.956)	0.875 (0.762 – 0.988)	0.858 (0.755 – 0.960)
Mean	0.928 (0.865 – 0.991)	0.925 (0.864 – 0.986)	0.930 (0.874 – 0.985)
All	0.898 (0.786 – 0.991)	0.868 (0.737 – 0.991)	0.878 (0.749 – 0.990)

For all pathologists and all morphometric parameters significance ( $p < 0.001$ ) was reached.

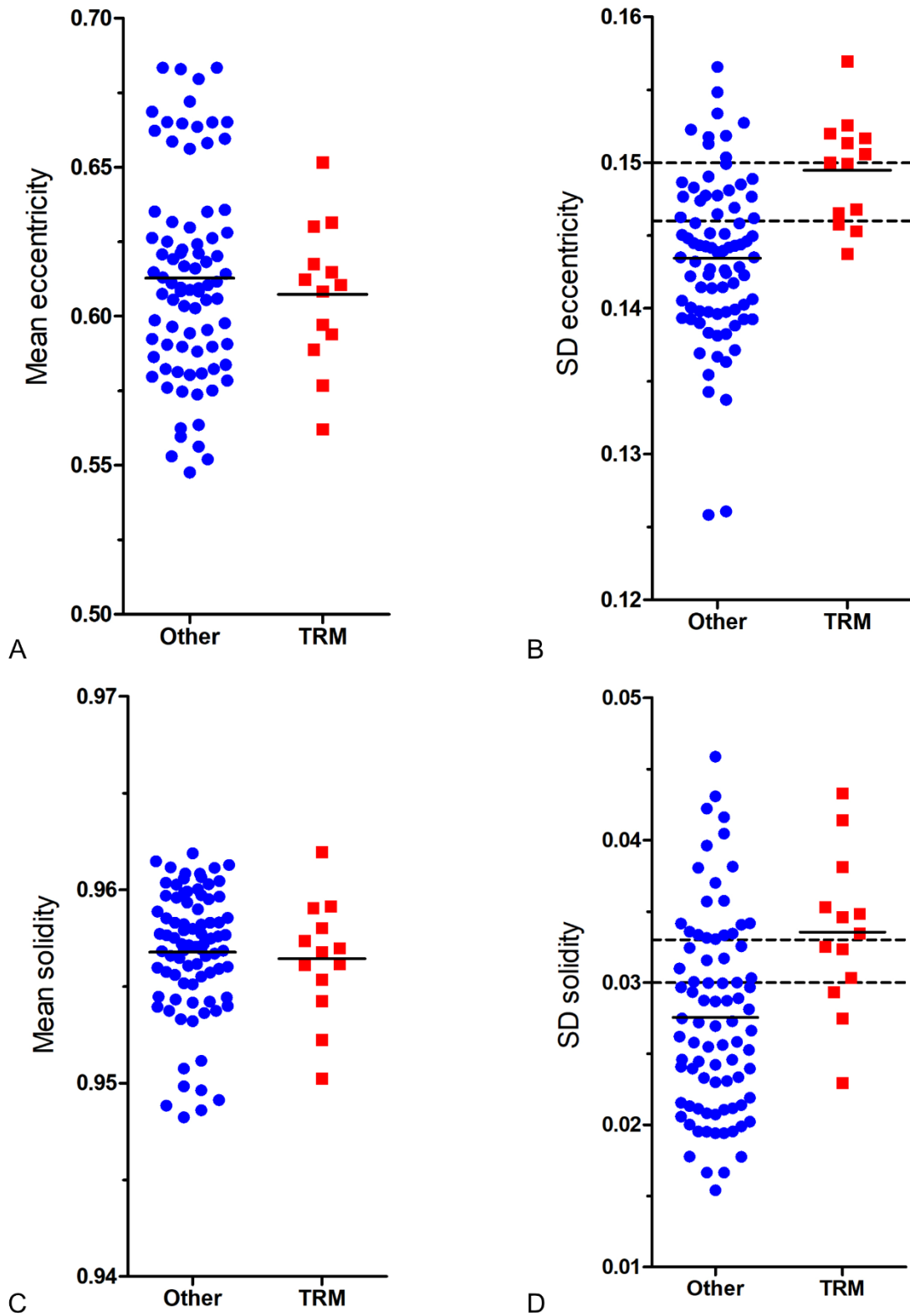
Mean, the mean of the measurements of the 9 pathologists per case was used to determine the AUC values.

All, combined data of all 9 pathologists (repeated measures) was used for analysis with bootstrapping.

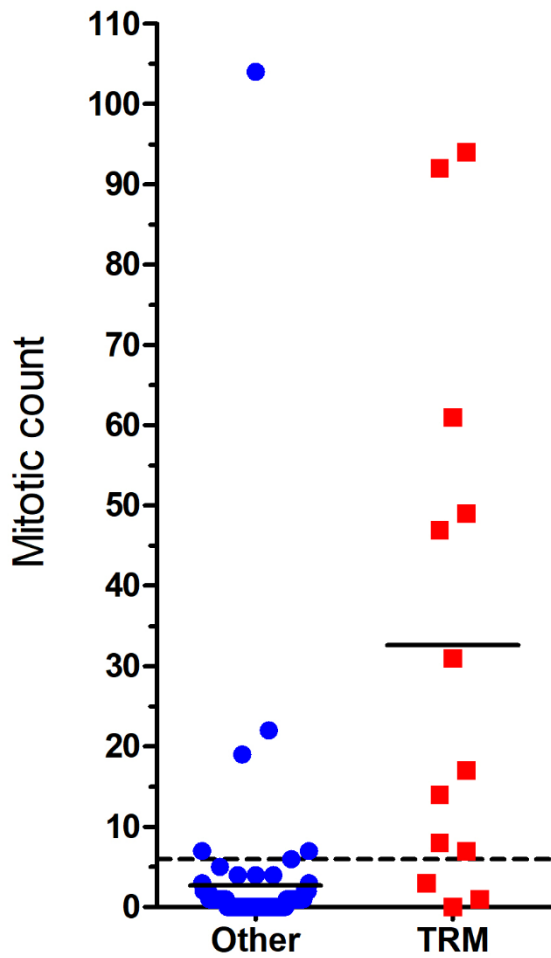
**Scatter plots**



**Supplemental Figure S6.** Scatterplots for area parameters of algorithmic nuclear morphometry comparing cases with tumor-related mortality (TRM) with others (survived observational period or died due to tumor-unrelated cause). The lower broken line represents threshold 1 and the upper broken line represents threshold 2 (see Supplemental table S8 and S9). The short solid lines represent the mean of the measurement of the respective outcome group. **A)** mean nuclear area in  $\mu\text{m}^2$ , **B)** standard deviation (SD) of nuclear area in  $\mu\text{m}^2$ , **C)** 90<sup>th</sup> percentile of nuclear area in  $\mu\text{m}^2$ , **D)** percentage (%) of large nuclei with an area  $>37.8 \mu\text{m}^2$ .



**Supplemental Figure S7.** Scatterplots for shape parameters of algorithmic nuclear morphometry comparing cases with tumor-related mortality with others (survived observational period or died due to tumor-unrelated cause). The lower broken line represents threshold 1 and the upper broken line represents threshold 2 (see Supplemental table S8 and S9). The short solid lines represent the mean of the measurement of the respective outcome group. **A)** Mean eccentricity **B)** SD of eccentricity, **C)** Mean solidity, **D)** SD of eccentricity.



**Supplemental Figure S8.** Scatterplot for the mitotic count (benchmark for this study) comparing cases with tumor-related mortality with others. The lower broken line represents the threshold proposed by Romansik et al. of  $MC \geq 6$  (Vet Pathol, 2007; DOI: 10.1354/vp.44-3-335). The short solid lines represent the mean of the measurement of the respective outcome group.

## Sensitivity and Specificity

**Supplemental Table S9.** Sensitivity, specificity, and precision (also known as positive predictive value) regarding tumor-related mortality for the different morphometric parameters of algorithmic nuclear morphometry using threshold 1.

Morphometric parameter	Threshold value	Sensitivity	Specificity	Precision
Mean area	27.0 $\mu\text{m}^2$	76.9%	86.7%	47.6%
Median area	27.5 $\mu\text{m}^2$	76.9%	91.6%	58.8%
SD of area	9.0 $\mu\text{m}^2$	76.9%	89.2%	52.6%
90 <sup>th</sup> percentile (90 <sup>th</sup> P)	38.7 $\mu\text{m}^2$	76.9%	90.4%	55.6%
90 <sup>th</sup> P / median	1.40	76.9%	79.5%	37.0%
Mean of the largest 10% of the nuclei	44.1 $\mu\text{m}^2$	76.9%	85.5%	45.5%
Percentage of large nuclei (>37.8 $\mu\text{m}^2$ )	11.5 %	76.9%	89.2%	52.6%
Percentage of large nuclei (>50.3 $\mu\text{m}^2$ )	2.4 %	76.9%	90.4%	55.6%
SD of eccentricity	0.146	76.9%	69.9%	28.6%
SD of solidity	0.030	76.9%	68.7%	27.8%

SD, standard deviation

**Supplemental Table S10.** Sensitivity, specificity, and precision (also known as positive predictive value) regarding tumor-related mortality for the different morphometric parameters of algorithmic nuclear morphometry using threshold 2.

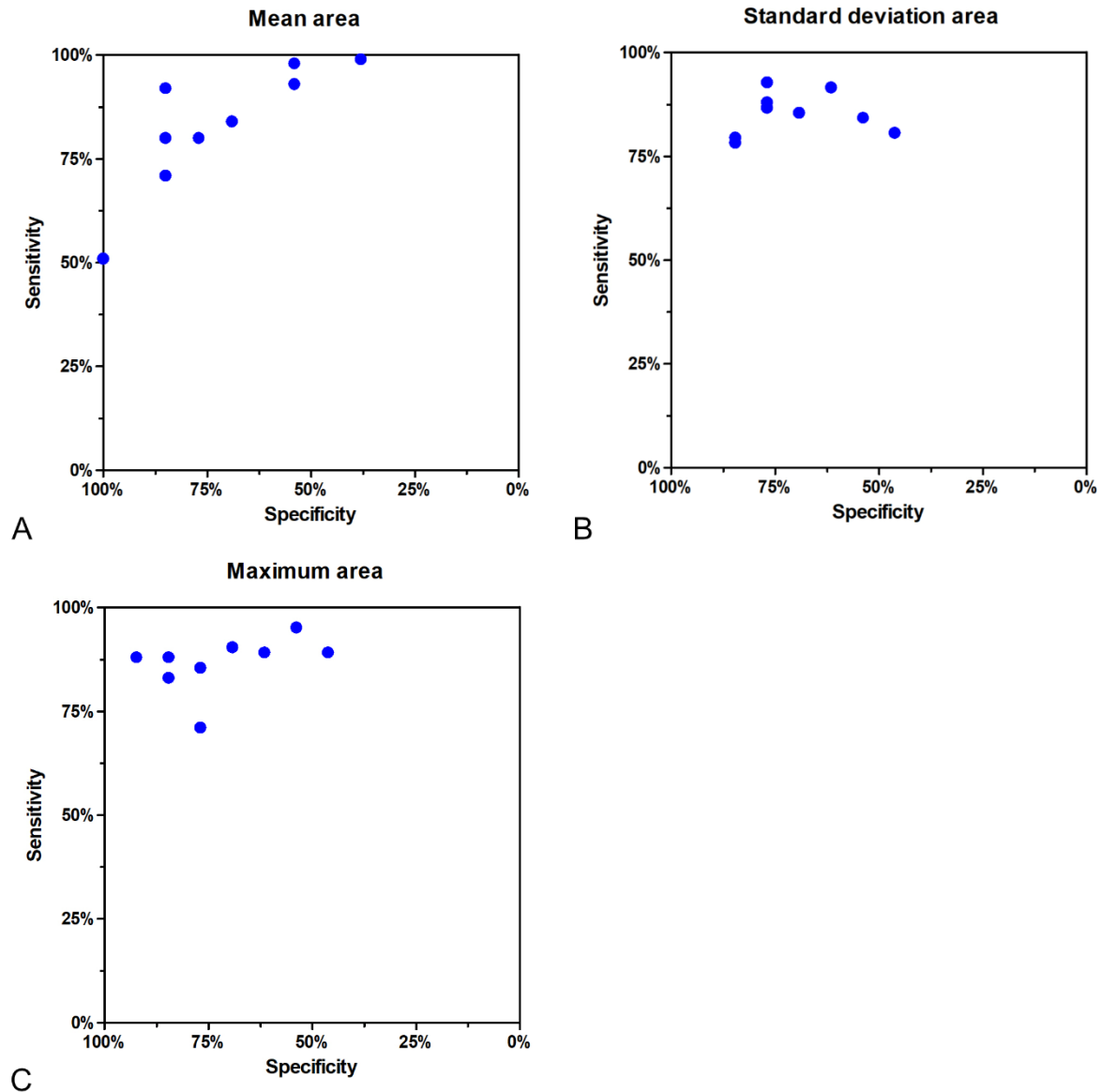
Morphometric parameter	Threshold value	Sensitivity	Specificity	Precision
Mean area	33.2 $\mu\text{m}^2$	53.8%	100%	100%
Median area	31.7 $\mu\text{m}^2$	53.8%	100%	100%
SD of area	11.5 $\mu\text{m}^2$	53.8%	100%	100%
90 <sup>th</sup> percentile (90 <sup>th</sup> P)	45.0 $\mu\text{m}^2$	53.8%	100%	100%
90 <sup>th</sup> P / median	1.44	53.8%	90.4%	46.7%
Mean of the largest 10% of the nuclei	53.9 $\mu\text{m}^2$	53.8%	100%	100%
Percentage of large nuclei (>37.8 $\mu\text{m}^2$ )	31.0 %	53.8%	100%	100%
Percentage of large nuclei (>50.3 $\mu\text{m}^2$ )	4.9 %	53.8%	100%	100%
SD of eccentricity	0.150	53.8%	89.2%	43.8%
SD of solidity	0.033	53.8%	78.3%	28.0%

SD, standard deviation

**Supplemental Table S11.** Sensitivity (Sen) and specificity (Sp) regarding tumor-specific mortality for the different morphometric parameters of manual nuclear morphometry using threshold 1. The threshold (thres.) was calculated from the mean pathologists' measurements of the 96 outcome cases.

Path-ologist	Mean area (thres.: 33.4 $\mu\text{m}^2$ )		SD of area (thres.: 10.9 $\mu\text{m}^2$ )		Maximum area (thres.: 54.9 $\mu\text{m}^2$ )	
	Sen	Sp	Sen	Sp	Sen	Sp
P1	84.6%	91.6%	61.5%	91.6%	69.2%	90.4%
P2	84.6%	79.5%	53.8%	84.3%	84.6%	88.0%
P3	38.5%	98.8%	76.9%	88.0%	53.8%	95.2%
P5	53.8%	92.8%	76.9%	72.3%	76.9%	85.5%
P6	53.8%	97.6%	46.2%	80.7%	46.2%	89.2%
P7	84.6%	71.1%	76.9%	92.8%	92.3%	88.0%
P8	69.2%	84.3%	69.2%	85.5%	61.5%	89.2%
P10	76.9%	79.5%	84.6%	79.5%	84.6%	83.1%
P11	100%	50.6%	84.6%	78.3%	76.9%	71.1%
Mean	76.9%	88.0%	76.9%	85.5%	76.9%	89.2%

Mean, the mean of the measurement of the 9 pathologists per case was used to determine the sensitivity and specificity values.



**Supplemental Figure S9.** Graphical comparison of the sensitivity and specificity values regarding tumor-related mortality for the different size parameters of manual nuclear morphometry. Each datapoint (blue dots) represents an individual pathologist. For case classification threshold 1 (based on the mean measurement of the 9 pathologists) was used (see Supplemental Table S10). **A)** Mean area (threshold: 33.4  $\mu\text{m}^2$ ), **B)** standard deviation of nuclear area (threshold: 10.9  $\mu\text{m}^2$ ), **C)** maximum area (threshold: 54.9  $\mu\text{m}^2$ ).



**Supplemental Table S12.** Sensitivity (Sen), specificity (Sp), and precision (Pre, also known as positive predictive value) regarding tumor-specific mortality for three-tier anisokaryosis estimates combining two of the three categories (1 = no to mild, 2 = moderate, 3 = severe).

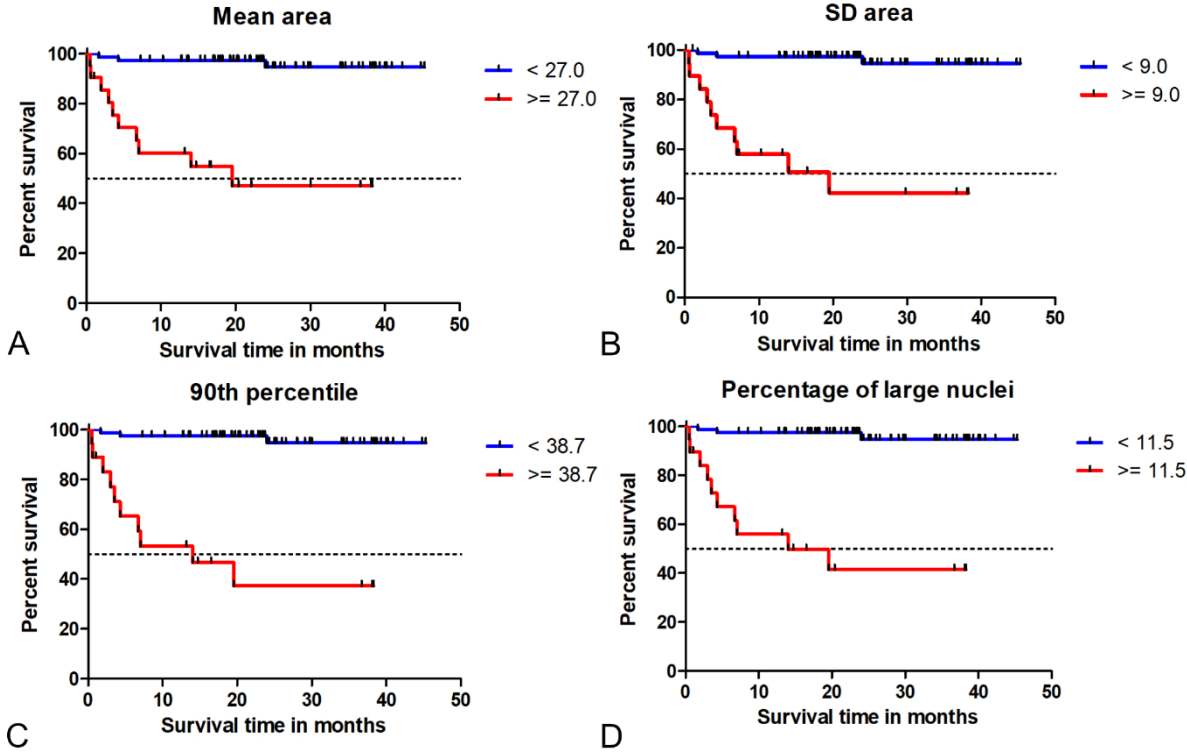
Path-ologist	Time point	Anisokaryosis 1 vs. 2+3			Anisokaryosis 1+2 vs. 3		
		Sen	Sp	Pre	Sen	Sp	Pre
P1	1	76.9%	85.5%	45.5%	0%	100%	NA
	2	61.5%	90.4%	50.0%	0%	100%	NA
P2	1	76.9%	48.2%	18.9%	38.5%	96.4%	62.5%
	2	69.2%	71.1%	27.3%	23.1%	95.2%	42.9%
P3	1	92.3%	49.4%	22.2%	46.2%	88.0%	37.5%
	2	92.3%	32.5%	17.6%	76.9%	84.3%	43.5%
P4	1	92.3%	51.8%	23.1%	61.5%	96.4%	72.7%
P5	1	84.6%	38.6%	17.7%	38.5%	86.7%	31.3%
	2	92.3%	19.3%	15.2%	84.6%	69.9%	30.6%
P6	1	69.2%	54.2%	19.1%	46.2%	95.2%	60.0%
	2	76.9%	60.2%	23.3%	30.8%	98.8%	80.0%
P7	1	46.2%	98.8%	85.7%	0%	100%	NA
	2	61.5%	89.2%	47.1%	0%	100%	NA
P8	1	100%	13.3%	15.3%	69.2%	90.4%	52.9%
	2	100%	4.8%	14.1%	76.9%	77.1%	34.5%
P9	1	46.2%	97.6%	75.0%	7.7%	100%	100%
P10	1	76.9%	66.3%	26.3%	53.8%	92.8%	53.8%
	2	53.8%	89.2%	43.8%	23.1%	98.8%	75.0%
P11	1	76.9%	78.3%	35.7%	30.8%	98.8%	80.0%
	2	61.5%	81.9%	34.8%	30.8%	100%	100%

NA, not available due to division by 0.

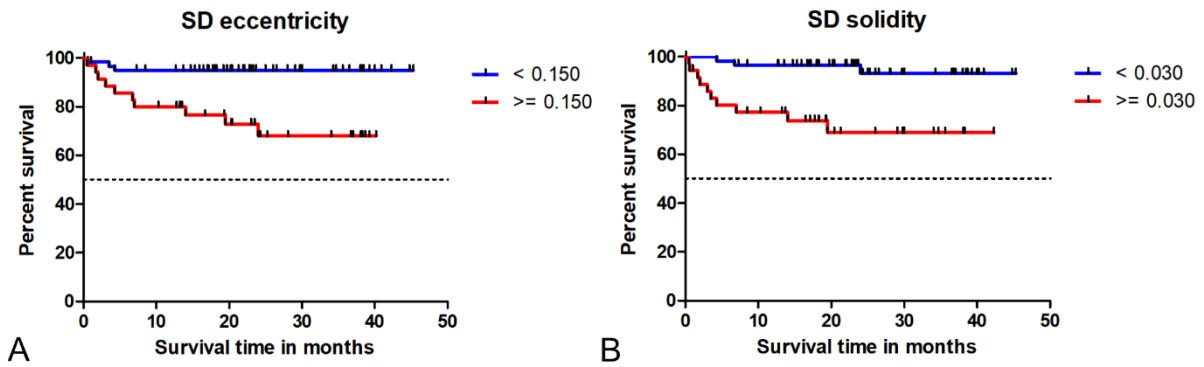
**Supplemental Table S13.** Sensitivity, specificity, and precision (also known as positive predictive value) regarding tumor-specific mortality for karyomegaly estimates.

Pathologist	Time point	Karyomegaly (presence vs. absence)		
		Sensitivity	Specificity	Precision
P1	1	38.5%	95.2%	55.6%
	2	15.4%	98.8%	66.7%
P2	1	61.5%	71.1%	25.0%
	2	46.2%	92.8%	50.0%
P3	1	30.8%	100%	100%
	2	38.5%	95.2%	55.6%
P4	1	46.2%	97.6%	75.0%
P5	1	0%	98.8%	0%
	2	30.8%	94.0%	44.4%
P6	1	69.2%	66.3%	24.3%
	2	69.2%	75.9%	31.0%
P7	1	23.1%	98.8%	75.0%
	2	23.1%	100%	100%
P8	1	69.2%	97.6%	81.8%
	2	69.2%	95.2%	69.2%
P9	1	76.9%	83.1%	41.7%
P10	1	76.9%	65.1%	25.6%
	2	53.8%	89.2%	43.8%
P11	1	92.3%	32.5%	17.6%
	2	92.3%	31.3%	17.4%

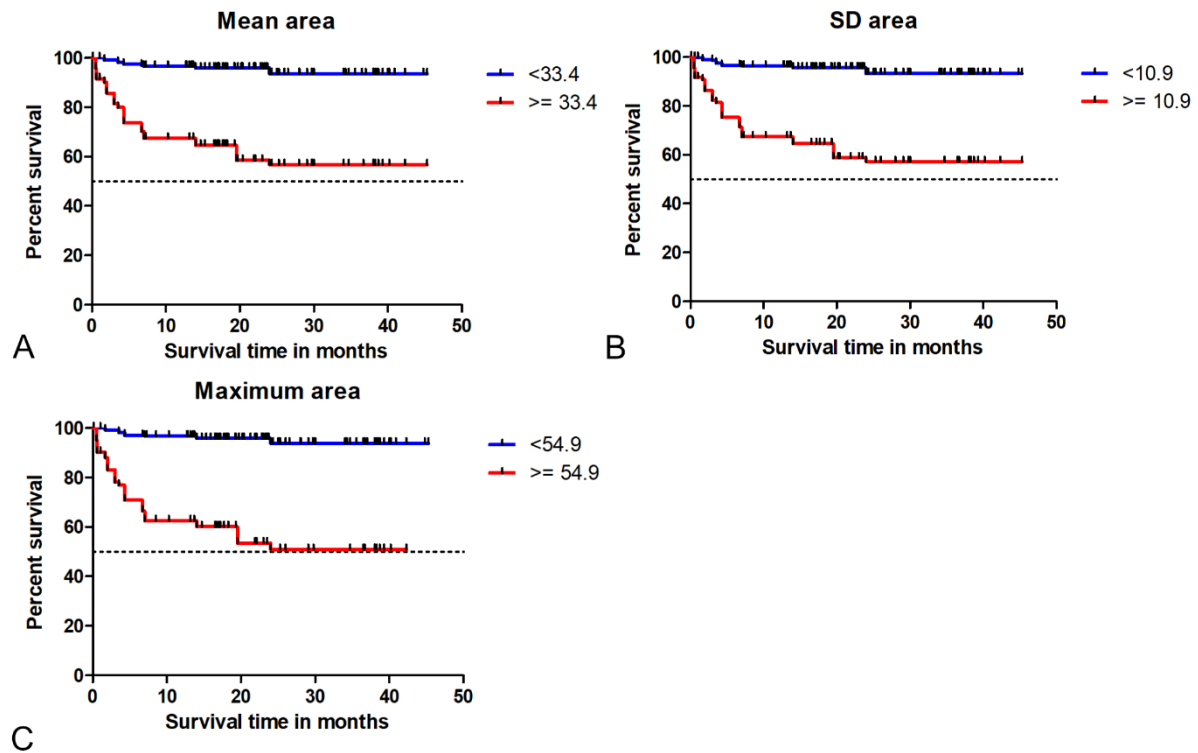
# Kaplan Meier Curves



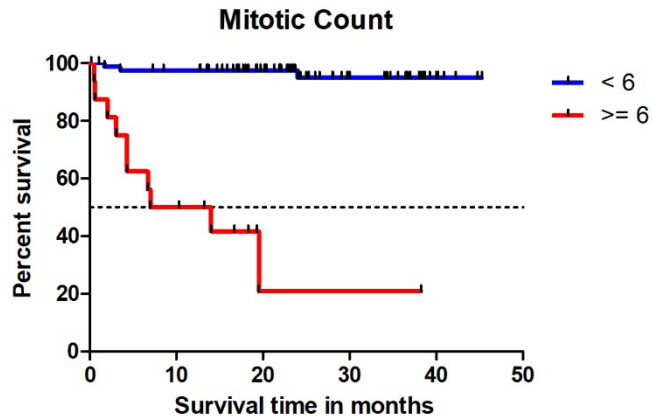
**Supplemental Figure S10.** Kaplan Meier curves and log rank tests regarding tumor-specific survival time for different size parameters of algorithmic nuclear morphometry. Cases are classified by threshold 1. **A)** mean nuclear area ( $p < 0.001$ ), **B)** standard deviation (SD) of nuclear area ( $p < 0.001$ ), **C)** 90<sup>th</sup> percentile of nuclear area ( $p < 0.001$ ), **D)** percentage of large nuclei with an area  $>37.8 \mu\text{m}^2$  ( $p < 0.001$ ).



**Supplemental Figure S11.** Kaplan Meier curves and log rank tests regarding tumor-specific survival time for different shape parameters of algorithmic nuclear morphometry. The combined data of all 9 pathologists were used and the log rank test was not provided due to repeated measures data. Cases are classified by threshold 1. **A**) Standard deviation (SD) of eccentricity ( $p = 0.0018$ ), **B**) SD of solidity ( $p < 0.001$ ).



**Supplemental Figure S12.** Kaplan Meier curves and log rank tests regarding tumor-specific survival time for different size parameters of manual nuclear morphometry. The combined data of all 9 pathologists were used and the log rank test is not provided due to repeated measures data. Cases are classified by threshold 1 based on the mean measurements of the pathologists. **A)** Mean area, **B)** standard deviation (SD) of area, **C)** Maximum area.



**Supplemental Figure S13.** Kaplan Meier curve regarding tumor-specific survival for the mitotic count (log rank test:  $p < 0.001$ ). Cases are classified by the threshold proposed by Romansik et al. (Vet Pathol, 2007; DOI: 10.1354/vp.44-3-335).

## Hazard Ratios (Univariate Cox Regression with Categorical Data)

**Supplemental Table S14.** Hazard ratios (HR) with 95% confidence intervals (95% CI) determined from univariate cox regression regarding tumor-specific survival time for the different morphometric parameters of algorithmic nuclear morphometry. Cases are dichotomized based on threshold 1.

Morphometric category	Morphometric parameter	Threshold 1	HR (95% CI)
Size (area in $\mu\text{m}^2$ )	Mean	27.0 $\mu\text{m}^2$	16.8 (4.5 – 61.4) **
	Median	27.5 $\mu\text{m}^2$	23.2 (6.3 – 85.0) **
	Standard deviation	9.0 $\mu\text{m}^2$	18.3 (5.0 – 67.1) **
	90 <sup>th</sup> percentile (90 <sup>th</sup> P)	38.7 $\mu\text{m}^2$	21.4 (5.8 – 78.5) **
	90 <sup>th</sup> P/ median	1.40	10.5 (2.8 – 38.4) **
	Mean of the largest 10% of the nuclei	44.1 $\mu\text{m}^2$	14.8 (4.0 – 54.1) **
	Percentage of large nuclei (>37.8 $\mu\text{m}^2$ )	11.5 %	19.5 (5.3 – 71.4) **
	Percentage of large nuclei (>50.3 $\mu\text{m}^2$ )	2.4 %	19.6 (5.3 – 71.9) **
Shape	SD of eccentricity	0.146	6.1 (1.6 – 22.1) *
	SD of solidity	0.030	6.7 (1.8 – 24.5) *

\*  $p \leq 0.05$ ; \*\*  $p \leq 0.001$

**Supplemental Table S15.** Hazard ratios with 95% confidence intervals determined from univariate cox regression regarding tumor-specific survival time for the different morphometric area parameters of manual nuclear morphometry. Cases are dichotomized by threshold 1 based on the mean measurements of the pathologists.

Pathologist	Mean area (threshold: $\mu\text{m}^2$ )	SD of area (threshold: $\mu\text{m}^2$ )	Maximum area (threshold: $\mu\text{m}^2$ )
P1	35.4 (7.7 – 160.9) **	12.5 (4.0 – 38.8) **	15.8 (4.7 – 51.9) **
P2	15.7 (3.4 – 71.0) **	4.8 (1.6 – 14.2) *	24.1 (5.3 – 108.9) **
P3	18.8 (6.0 – 58.6) **	15.0 (4.1 – 54.7) **	13.6 (4.5 – 40.7) **
P5	10.5 (3.5 – 31.5) **	6.9 (1.8 – 25.0) *	13.0 (3.5 – 47.2) **
P6	19.9 (6.5 – 60.0) **	3.3 (1.1 – 9.8) *	5.5 (1.86 – 16.6) *
P7	11.5 (2.5 – 51.8) *	27.8 (7.5 – 102.7) **	63.1 (8.1 – 488.7) **
P8	9.4 (2.8 – 30.5) **	9.2 (2.8 – 29.7) **	8.8 (2.8 – 27.0) **
P10	10.6 (2.8 – 38.6) **	15.0 (3.3 – 67.6) **	18.7 (4.1 – 84.5) **
P11	56.6 (0.64 – ND)	15.0 (3.3 – 67.6) **	6.9 (1.90 – 25.3) *
Mean	17.1 (4.7 – 62.6) **	13.1 (3.6 – 47.6) **	16.9 (4.6 – 61.5) **
All	13.7 (8.9 – 21.2) **	9.0 (6.0 – 13.4) **	12.0 (8.0 – 18.0) **

\*  $p \leq 0.05$ ; \*\*  $p \leq 0.001$

SD, standard deviation

ND, not determined as statistical model did not converge

Mean, the mean of the measurements of the 9 pathologists per case was used to determine the HR values.

All, combined data of all 9 pathologists (repeated measures) was used for analysis with a mixed model.



**Supplemental Table S16.** Hazard ratios with 95% confidence intervals determined from univariate cox regression regarding tumor-specific survival time for the three-tier anisokaryosis (combined to two categories; 1 = no to mild, 2 = moderate, 3 = severe) and karyomegaly (presence vs. absence) estimates from time point 1.

Path-ologist	Three-tier anisokaryosis		Karyomegaly
	1 vs. 2+3	1+2 vs. 3	
P1	15.4 (4.2 – 56.4) **	NA	8.3 (2.7 – 25.8) **
P2	3.0 (0.82 – 10.9)	11.4 (3.7 – 35.4) **	3.6 (1.16 – 10.9) *
P3	10.1 (1.31 – 77.9) *	5.2 (1.74 – 15.5) *	19.5 (5.8 – 65.5) **
P4	11.9 (1.54 – 91.4) *	21.5 (6.9 – 66.6) **	15.7 (5.1 – 47.5) **
P5	3.1 (0.69 – 14.0)	3.3 (1.07 – 10.1) *	0.49 (0 – ND)
P6	2.4 (0.74 – 7.8)	11.1 (3.6 – 33.2) **	3.7 (1.15 – 12.1) *
P7	24.2 (7.6 – 76.8) **	NA	12.9 (3.4 – 48.3) **
P8	25.6 (0.26 – ND)	13.5 (4.1 – 44.2) **	27.5 (8.3 – 90.3) **
P9	16.3 (5.4 – 49.3) **	7.6 (0.98 – 58.8)	12.7 (3.4 – 46.4) **
P10	5.9 (1.61 – 21.4) *	11.2 (3.7 – 33.9) **	5.6 (1.5 – 20.2) *
P11	10.3 (2.8 – 37.5) **	11.6 (3.5 – 37.8) **	5.5 (0.71 – 42.6)

\*  $p \leq 0.05$ ; \*\*  $p \leq 0.001$

ND, not determined as statistical model did not converge

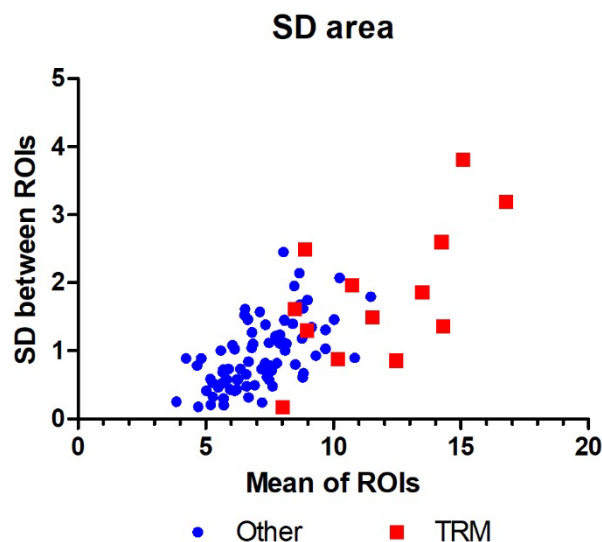
NA, not available as no category 3 anisokaryosis was determined by this pathologist.

## Heterogeneity between tumor regions

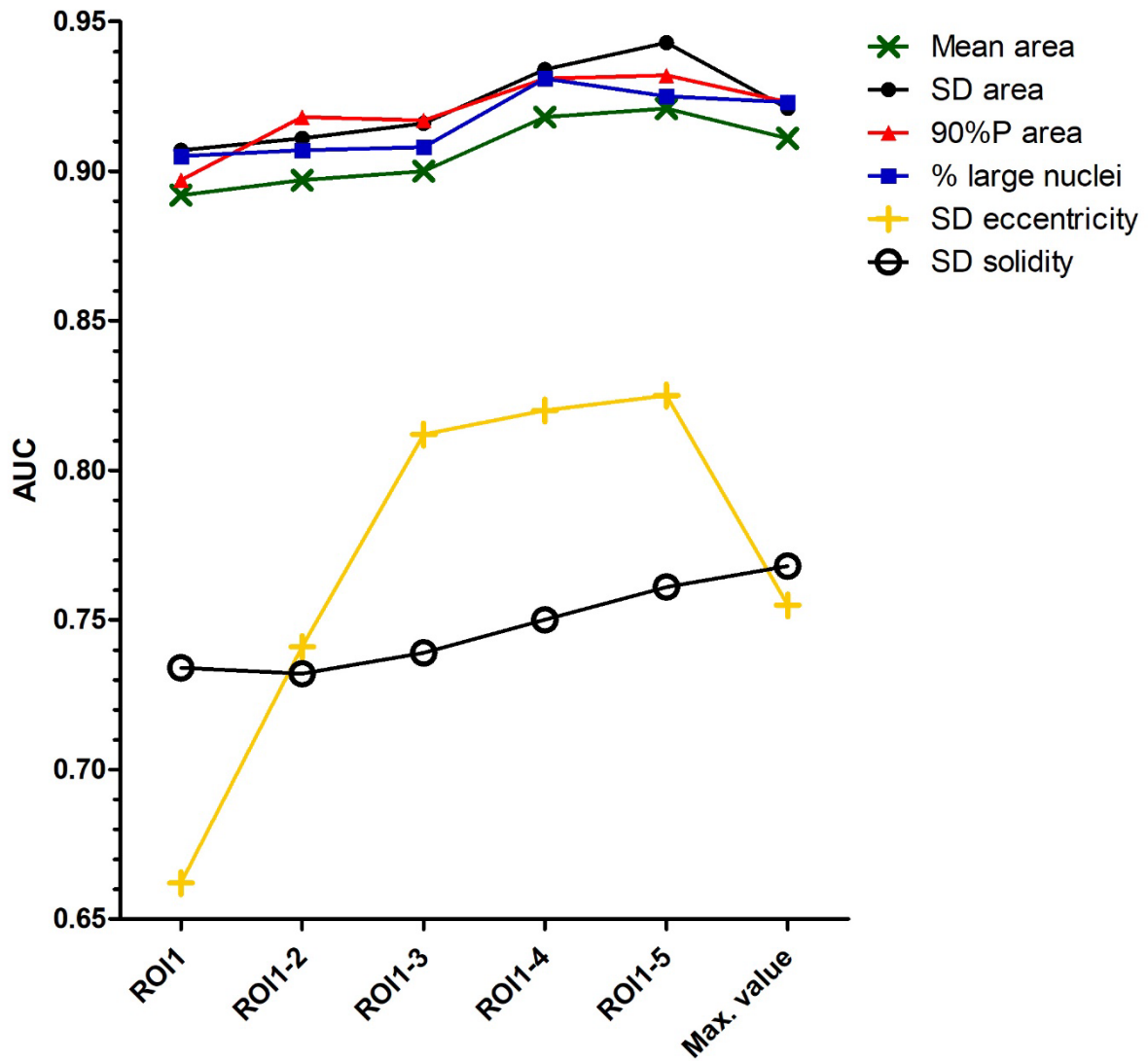
**Supplemental Table S17.** Summary of the coefficient of variation (standard deviation / mean) for the measurements in the 3-5 ROI comparing the different parameters of algorithmic morphometry.

Category	Morphometric parameter	Coefficient of variation	
		Mean of all cases	Range
Size (area in $\mu\text{m}^2$ )	Mean	8.3%	1.4 – 17.5%
	Standard deviation	13.3%	2.2 – 30.5%
	90 <sup>th</sup> percentile	8.9%	1.2 – 21.1%
	Mean of the largest 10% of the nuclei	10.4%	1.6 – 23.2%
	Percentage of large nuclei ( $>37.8 \mu\text{m}^2$ )	65.2% *	6.9% - 164.5% *
Shape	SD of eccentricity	4.2%	0.6 – 11.0%
	SD of solidity	17.2%	3.0 – 17.2%

\* The high coefficient of variation is mostly caused by absolute differences of a few percentages between the ROI in cases with low values ( $<5\%$ ) on average (resulting in high relative difference).



**Supplemental Figure S14.** Scatterplot for algorithmic morphometry of the standard deviation of the nuclear area comparing the mean values and the standard deviation between 5 tumor regions of interest (ROI). The red squares represent cases with tumor-related mortality (TRM) throughout the entire follow-up period and the blue dots represent cases without TRM.



**Supplemental Figure S15.** Line diagram of the area under the curve (AUC) values regarding tumor-related mortality (throughout the entire follow-up period) for different parameters of algorithmic morphometry comparing the number of tumor regions of interest (ROI) used for statistical analysis. An increasing number of ROI (1-5 according to their order of selection) was included. The maximum (max.) value represents the one ROI with the highest measurement of the 5 ROI.

**Supplemental Table S18.** AUC values for tumor heterogeneity as a prognostic test for tumor-specific survival using different parameters of algorithmic morphometry.

<b>Morphometric parameter</b>	<b>Area under the curve (95% confidence interval)</b>	
	<b>SD between ROI</b>	<b>Proportion of hotspots</b>
Mean area	0.606 (0.415 – 0.798)	0.890 (0.780 – 0.999) **
SD of area	0.790 (0.632 – 0.947) **	0.890 (0.780 – 1.00) **
90 <sup>th</sup> percentile	0.696 (0.521 – 0.871) *	0.918 (0.817 – 1.00) **
Mean of the largest 10% of the nuclei	0.759 (0.602 – 0.916) **	0.899 (0.789 – 1.00) **
Percentage of large nuclei (>37.8 $\mu\text{m}^2$ )	0.867 (0.760 – 0.975) **	0.911 (0.809 – 1.00) **
SD of eccentricity	0.554 (0.390 – 0.718)	0.814 (0.722 – 0.905) **
SD of solidity	0.683 (0.545 – 0.821) *	0.739 (0.623 – 0.855) **

\*  $p \leq 0.05$ ; \*\*  $p \leq 0.001$